JOURNAL OF PETROLOGY | VOLUME 45 | NUMBER 12 | PAGES 2507–2530 | 2004 | doi:10.1093/petrology/egh039

Geodynamic Information in Peridotite Petrology

CLAUDE HERZBERG*

DEPARTMENT OF GEOLOGICAL SCIENCES, RUTGERS UNIVERSITY, NEW BRUNSWICK, NJ 08903, USA

RECEIVED SEPTEMBER 10, 2003; ACCEPTED APRIL 21, 2004
ADVANCE ACCESS PUBLICATION AUGUST 5, 2004

Systematic differences are observed in the petrology and major element geochemistry of natural peridotite samples from the sea floor near oceanic ridges and subduction zones, the mantle section of ophiolites, massif peridotites, and xenoliths of cratonic mantle in kimberlite. Some of these differences reflect variable temperature and pressure conditions of melt extraction, and these have been calibrated by a parameterization of experimental data on fertile mantle peridotite. Abyssal peridotites are examples of cold residues produced at oceanic ridges. High-MgO peridotites from the Ronda massif are examples of hot residues produced in a plume. Most peridotites from subduction zones and ophiolites are too enriched in SiO_2 and too depleted in Al_2O_3 to be residues, and were produced by melt–rock reaction of a precursor protolith. Peridotite xenoliths from the Japan, Cascades and Chile–Patagonian back-arcs are possible examples of arc precursors, and they have the characteristics of hot residues. Opx-rich cratonic mantle is similar to subduction zone peridotites, but there are important differences in FeO_T. Opx-poor xenoliths of cratonic mantle were hot residues of primary magmas with 16–20% MgO, and they may have formed in either ancient plumes or hot ridges. Cratonic mantle was not produced as a residue of Archean komatiites.

KEY WORDS: *peridotite; residues; fractional melting; abyssal; cratonic mantle; subduction zone; ophiolite; potential temperature; plumes; hot ridges*

INTRODUCTION

Samples of peridotite from the Earth's mantle occur as xenoliths in kimberlite and alkali basalt, tectonic crustal emplacements (i.e. Alpine, orogenic, massif and seamount peridotite), and abyssal peridotite dredged from oceanic spreading centers. Observed mineralogical and geochemical variations have been interpreted to reflect magma removal followed by metasomatism (e.g. Maaloe & Aoki, 1977; Frey & Prinz, 1978; Herzberg, 1993; Parkinson & Pearce, 1998; Downes, 2001). Metasomatism can affect both trace and major element abundances (Parkinson & Pearce, 1998; Downes, 2001), but only the latter will be considered in this paper.

The major element composition of residual peridotite depends on both the amount and the composition of the melt extracted, relative to more fertile peridotite, and these depend on the geodynamic environment in which they form. For example, hot mantle peridotite at high potential temperatures appropriate to hotspots will begin to melt deeper and sometimes more extensively than colder mantle, which melts below oceanic ridges. Relative to basalts that characterize oceanic ridges, primary magmas that form at hotspots tend to be enriched in MgO and FeO and depleted in Al_2O_3; they solidify to rocks called picrites and komatiites. Mass balance requires that extraction of primary magmas with a wide range of compositions must leave behind residues that reflect this diversity. Partial melting processes must, therefore, account for at least some of the variability in the major element geochemistry and petrology of mantle peridotites. It would clearly be desirable if this process could be inverted to allow extraction of geodynamic information from the petrology of mantle peridotite samples.

Liquid compositions produced in controlled melting experiments on fertile mantle peridotite (KR-4003; Walter, 1998) at a wide range of pressures offer new possibilities for constraining the geochemistry of its melting residues. KR-4003 is a fertile peridotite (Walter, 1998) that can be modeled by about 1% mid-ocean ridge basalt (MORB) extraction from the primitive McDonough & Sun (1995) composition. Liquid compositions produced in these experiments were modeled with mass balance equations that are appropriate for both equilibrium and fractional melting at mass fractions of melting that span the 0·0–1·0 range (Herzberg &

*E-mail: Herzberg@rci.rutgers.edu

O'Hara, 2002). Results previously reported for FeO and MgO have been extended to Al_2O_3 and SiO_2 in this paper. The compositions of complementary residues produced by both equilibrium and fractional melting have been modeled by mass balance. These are then compared with natural peridotite samples from the sea floor near oceanic ridges and subduction zones, the mantle section of ophiolites, massif peridotites, and xenoliths of cratonic mantle in kimberlite. It will be shown that peridotite residues produced in geodynamic environments that differ in potential temperature can often be distinguished, but complexities can occur owing to subsequent stages of melt–rock reaction and addition of cumulus minerals.

Komatiites of Archean age left behind residues whose lithological identity is important for a comprehensive understanding of their origin. An examination is made of the mass balance requirements of computed residues of Archean komatiites with the goal of testing the commonly accepted theory that they are similar to kimberlite-hosted xenoliths of cratonic mantle. This paper concludes with an identification of the FeO_T and MgO contents of primary magmas that are complementary to residues of mantle peridotite, and these are compared with primary magmas that have been estimated for MORB and various hotspot occurrences. It is shown that many samples of cratonic mantle of Archean and Proterozoic ages are likely to be hot residues of picritic primary magmas that are similar in composition to those forming below Hawaii today.

RESIDUAL MANTLE PERIDOTITE

Model residue compositions of fertile mantle peridotite

For the limiting case of equilibrium melting, residue compositions were computed by mass balance from equilibrium liquid compositions of fertile peridotite KR-4003 (Herzberg & O'Hara, 2002); further details are given in Electronic Appendix 1 (available at http:www.petrology.oupjournals.org). For the case of accumulated fractional melting, the primary magma has a unique residue, but the accumulated liquid is not in equilibrium with that residue; only the final drop of liquid extracted is in equilibrium with the residue. Computed FeO and MgO contents of residues that develop during decompression fractional melting were not reported by Herzberg & O'Hara (2002), but are discussed in Electronic Appendix 1 and illustrated in Fig. 1a. Computed Al_2O_3 and SiO_2 contents of liquids and residues were also not given by Herzberg & O'Hara (2002); they are, however, given in Electronic Appendix 1 and Fig. 1b and c.

Peridotite residue compositions are important functions of the pressures of initial and final decompression melting. At constant MgO, increasing pressure of initial melting will produce residues that are lower in FeO (Fig. 1a), higher in Al_2O_3 (Fig. 1b) and higher in SiO_2 (Fig. 1c). When the pressure of initial melting is 2–3 GPa, residues can be strongly depleted in Al_2O_3 but remain unchanged in FeO. At very high pressures of initial melting, in the 7–10 GPa range, residues can be depleted or enriched in Al_2O_3, depending on the amount of melt extracted. Melt fraction increases when the pressure of final melting decreases, and this is universally reflected in residues with elevated MgO. Residues almost always have lower SiO_2 than the source.

Composition fields for harzburgite and dunite residues at magmatic conditions are also shown in Fig. 1. Additionally, there are numerous residue lithologies with compositions that plot between those for the peridotite source and harzburgite. These are typically spinel and garnet lherzolites, but include lherzolites, garnet harzburgites, and an assemblage with low-Ca pigeonitic clinopyroxene (L + Ol + low-Ca Cpx + Gt) (Herzberg & O'Hara, 2002). Natural peridotite samples typically have petrographic characteristics that correspond to those defined by the compositional fields in Fig. 1. However, small amounts of clinopyroxene, spinel, or garnet observed in peridotites that plot within the field defined by harzburgite can be of exsolution or metasomatic origin (Cox *et al.*, 1987; Boyd *et al.*, 1997).

The pressure at which melting begins increases with rising mantle potential temperature (e.g. McKenzie & Bickle, 1988), and two hypothetical cases are illustrated in Fig. 2a. One is for cold mantle that has a potential temperature of 1320°C and intersects the anhydrous solidus at 2 GPa. The other is an example of hot mantle that has a potential temperature of 1600°C and a pressure of initial melting at 5 GPa. For each case, fractional melting terminates at three pressures indicated by the closed circles, chosen to illustrate residue lithology and composition. Each closed circle in Fig. 2b shows the MgO and Al_2O_3 contents of the simulated residue produced at the conditions of melting shown in Fig. 2a. The three residues produced at each potential temperature define a simple array that is coincident with a line of initial melting pressure. Although the simulation in Fig. 2a is shown only for MgO–Al_2O_3, similar arrays must be observed in MgO–FeO and MgO–SiO_2 space. In the following sections, the simulated residues in Fig. 2 are replaced with the contents of MgO, FeO, Al_2O_3, and SiO_2 in naturally occurring peridotite samples to infer pressures of melting and melt fractions, information that is used to constrain mantle potential temperature. Arrays of peridotite compositions that do not plot along common initial melt pressure lines when viewed in combined MgO–SiO_2, MgO–Al_2O_3, and MgO–FeO space cannot be simple residues of fertile peridotite KR-4003. Examples will be discussed in the following sections.

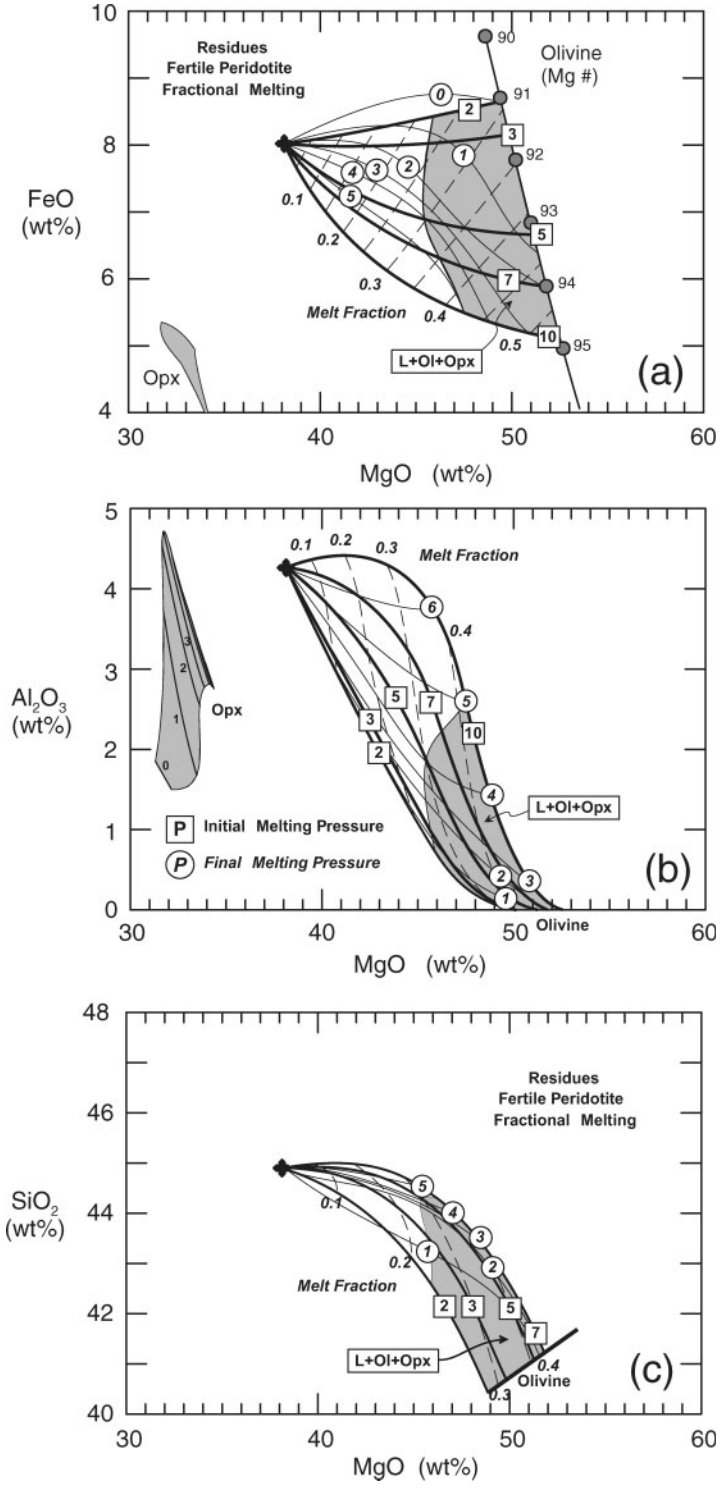

Fig. 1. Model residue compositions formed by fractional melting of fertile peridotite KR-4003. Line labelled 90–95 in (a) shows *mg*-numbers of olivine. Gray shaded fields are compositions of residual harzburgite designated as [L + Ol + Opx]. Light shaded fields bounded by the field of harzburgite residues and the bulk composition (bold cross) are various spinel or garnet peridotite assemblages. Bold lines labelled with squares, initial melting pressures in GPa; light lines labelled with circles, final melting pressures; light dashed lines, melt fractions. [See Electronic Appendix 1 (http:www.petrology.oup-journals.org) for discussion.] Orthopyroxene compositions are from Herzberg & O'Hara (2002) for liquids in equilibrium with harzburgite at the pressures (GPa) indicated in (b).

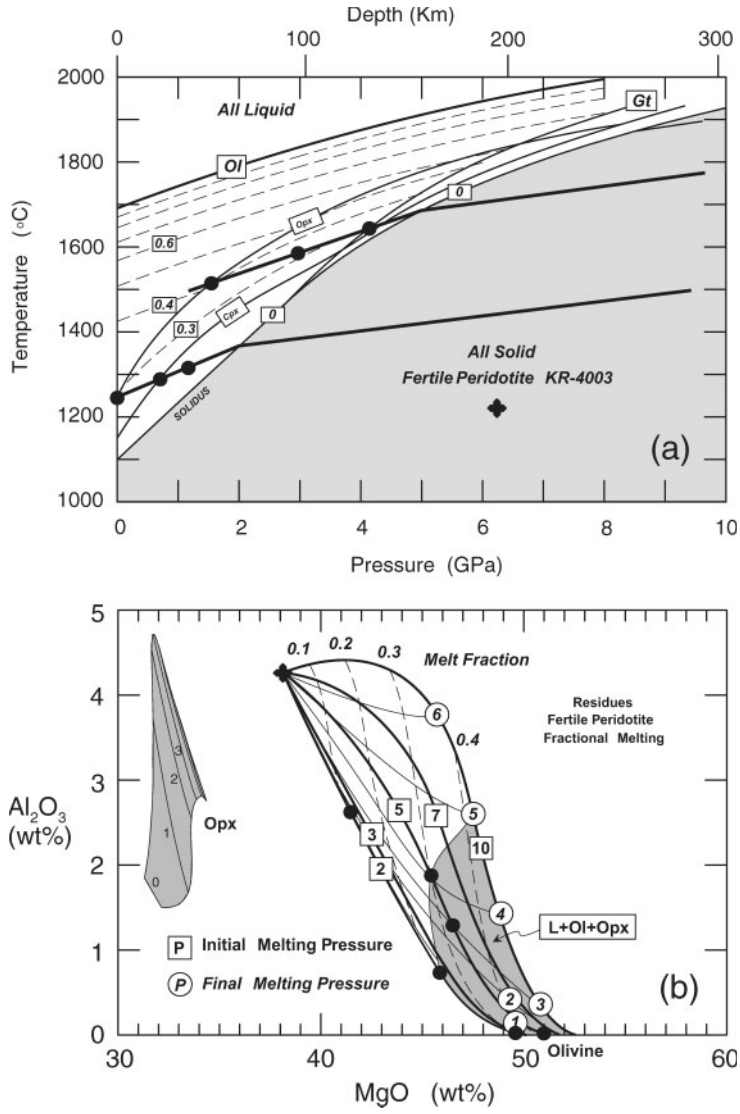

Fig. 2. An example showing how Al_2O_3 and MgO contents of peridotite residues are related to mantle temperatures and pressures of fractional melting. (a) *T*–*P* diagram from Herzberg & O'Hara (2002). Absolute temperatures and pressures are approximate because they are strictly valid for equilibrium melting. The effect of fractional melting is to produce higher liquidus crystallization temperatures. Subsolidus adiabatic gradients are from Iwamori *et al.* (1995) and Herzberg & O'Hara (2002). Supersolidus adiabatic gradients have been given by Herzberg & O'Hara (2002, fig. 13). •, pressures at which fractional melting stops (i.e. final melting pressures). For cold mantle at a mantle potential temperature of 1320°C, initial melting occurs at 2 GPa and melting stops at three pressures, forming residues of spinel lherzolite, harzburgite, and dunite. For hot mantle at a mantle potential temperature of 1600°C, initial melting occurs at 5 GPa and melting stops at three pressures, forming two different residues of harzburgite and dunite. (b) Residue compositions corresponding to final melting pressures in (a), from Fig. 1b. Bold lines labelled with squares, initial melting pressures; light lines labelled with circles, final melting pressures; light dashed lines, melt fractions; gray shaded fields, compositions of residual harzburgite designated as [L + Ol + Opx].

Observed mantle peridotite samples: treatment of data, assumptions, limitations

A brief survey is made of relatively young peridotites as a prelude to an evaluation of cratonic peridotites of Archean age. 'Young' refers to peridotites from modern ocean basins (abyssal peridotites), Tethyan ophiolites, and the Ronda orogenic massif. Although obduction and emplacement ages are usually young, Proterozoic Re–Os ages have been reported, considered to reflect a magmatic depletion event (e.g. Reisberg & Lorand, 1995).

With the exception of peridotites from subduction zones, reported values of FeO_T are recalculated to

Fe_2O_3 and FeO using the relation

$$Fe^{3+}/\Sigma Fe = (14{\cdot}7 - 0{\cdot}3MgO)/100 \quad (1)$$

as empirically determined by Canil *et al.* (1994) for a wide range of peridotite samples. In most cases, recalculated FeO contents, rather than FeO_T, are plotted in Fig. 1a even though the computed Fe_2O_3 content is usually very small. The reason for making this distinction is because the FeO contents displayed in Fig. 1a were computed strictly for iron that is exchangeable between olivine and liquid, i.e. Fe^{2+} (Herzberg & O'Hara, 2002). Whole-rock peridotite analyses were normalized to 100% anhydrous, and FeO and MgO are plotted in Fig. 1a. Subduction zone peridotites might have considerably more Fe_2O_3 than that calculated from equation (1), and this is discussed below.

All interpretations concerning the pressure of initial and final melting extracted from Fig. 1 assume that the initial source had a composition similar to that of fertile peridotite (i.e. KR-4003; 44·90% SiO_2, 4·26% Al_2O_3, 8·02% FeO, 38·12% MgO). This assumption will be repeatedly tested by combining plots of residue compositions in MgO–SiO_2, MgO–Al_2O_3, and MgO–FeO space.

Unless stated otherwise, a comparison is made of the compositions of observed mantle peridotites with computed residues expected from fractional melting of fertile peridotite rather than equilibrium melting (e.g. McKenzie, 1984; Johnson *et al.*, 1990). However, abyssal peridotite residues are compared with residues expected from both equilibrium and fractional melting, and this is discussed in the following section.

Abyssal peridotites

Abyssal peridotites are fragments of mantle that have been dredged from modern ocean basins (e.g. Dick & Fisher, 1984; Dick, 1989; Johnson & Dick, 1992). Serpentinization is pervasive and whole-rock chemical analysis is compromised (Snow & Dick, 1995). Original whole-rock compositions are reconstructed using primary mineral modes and either analyzed (Dick & Fisher, 1984; Dick, 1989) or calculated (Niu, 1997; Baker & Beckett, 1999) phase compositions. The common database presented by Dick and coworkers has resulted in two very different model whole-rock reconstructions (Niu, 1997; Baker & Beckett, 1999) owing to different assumptions in calculated phase compositions.

The Baker & Beckett (1999) model abyssal peridotite compositions define trends that are mostly coincident with residues of fertile peridotite produced by fractional melting in combined MgO–SiO_2, MgO–Al_2O_3, and MgO–FeO space (Fig. 3). Inferred initial melting pressures are 2–3 GPa, final melting pressures are 0·5–2·0 GPa, and melt fractions ranged from 0·09 to 0·25. They are also similar to residues produced by equilibrium melting as discussed in Electronic Appendix 2 on the *Journal of Petrology* website (http:www.petrology.oupjournals.org). These similarities do not permit a conclusion to be drawn about the relative importance of equilibrium vs fractional melting (Electronic Appendix 2). The Niu (1997) model defines a trend that is positively correlated in FeO–MgO space (Fig. 3a), inconsistent with a trend expected of simple residues (see discussion of Fig. 2). Niu (1997) and Niu *et al.* (1997) interpreted the model abyssal peridotites as residues into which cumulus olivine was later added by partial crystallization of MORB. Both models are nearly coincident with residues at initial melting pressures of 2–3 GPa when viewed in MgO–Al_2O_3 space, but possible olivine addition is revealed by low SiO_2 and Al_2O_3 contents in some cases (Fig. 3b and c). More recent data by Seyler *et al.* (2003) are consistent with both interpretations (Fig. 3). Fractional melting cannot account for elevated TiO_2 and Na_2O in abyssal peridotites, a matter that has received considerable attention elsewhere (Elthon, 1992; Asimow, 1999; Baker & Beckett, 1999; Niu & O'Hara, 2003).

Pressures of initial melting of 2–3 GPa obtained here are similar to other estimates for abyssal peridotite (Asimow, 1999), and for MORB generation (McKenzie & Bickle, 1988; Langmuir *et al.*, 1992; Asimow *et al.*, 2001; Herzberg & O'Hara, 2002). Using the *T*–*P* diagram in Fig. 2a and adiabatic gradients given by Iwamori *et al.* (1995) and Herzberg & O'Hara (2002), the potential temperatures can be inferred to be 1300–1450°C, in good agreement with 1280–1400°C for most MORB estimates (Herzberg *et al.*, submitted). These potential temperatures are relatively cold compared with plume occurrences (Herzberg & O'Hara, 2002). Residues of abyssal peridotite are therefore considered 'cold'.

Peridotites from the Ronda massif

Whole-rock data for peridotites from the Ronda orogenic massif (Frey *et al.*, 1985) define trends that are coincident with model residues formed by initial melting at 2–5 GPa and final melting at 1–2 GPa (Fig. 4). Misfits occur for samples that have been contaminated by mafic layers (Frey *et al.*, 1985), and unpublished data indicate that modification of bulk-rock *mg*-number is also possible by infiltration metasomatism or melt–rock reaction (Bedini *et al.*, 2003; J. L. Bodinier, personal communication, 2004). Inferred melt fractions from Fig. 4 are 0–0·30, in excellent agreement with previous estimates (Frey *et al.*, 1985). Samples from Ronda with the highest MgO contents exhibit the highest pressures of initial melting (i.e. P_o = 3–5 GPa; Fig. 4a–c). Inferred potential temperatures range from about 1450 to 1550°C (Fig. 2a), hotter than abyssal peridotites. These residues are therefore considered 'hot'. Samples with the lowest MgO contents

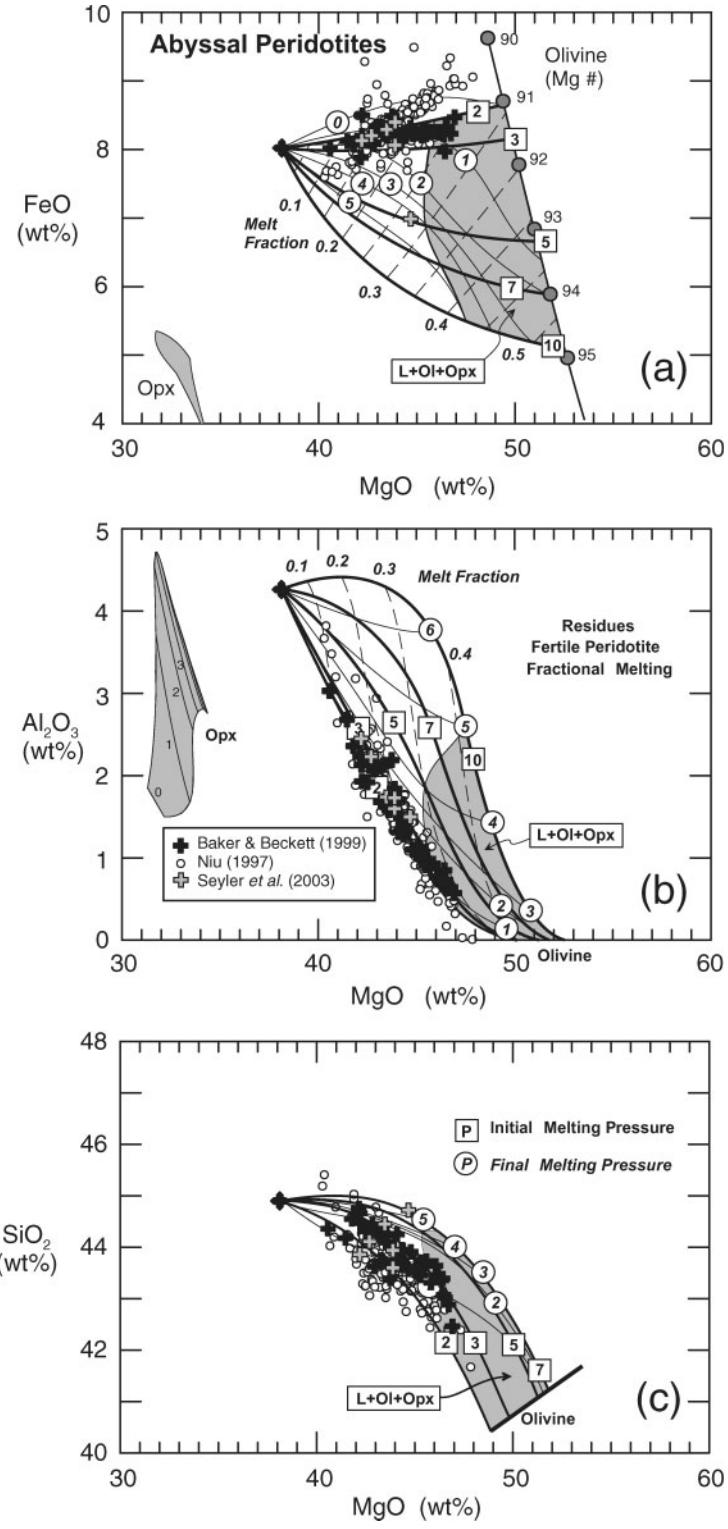

Fig. 3. Abyssal peridotite compositions compared with model residues formed by fractional melting of fertile peridotite KR-4003. Bold lines labelled with squares, initial melting pressures; light lines labelled with circles, final melting pressures; light dashed lines, melt fractions; gray shaded fields, compositions of residual harzburgite designated as [L + Ol + Opx]. Data sources are indicated.

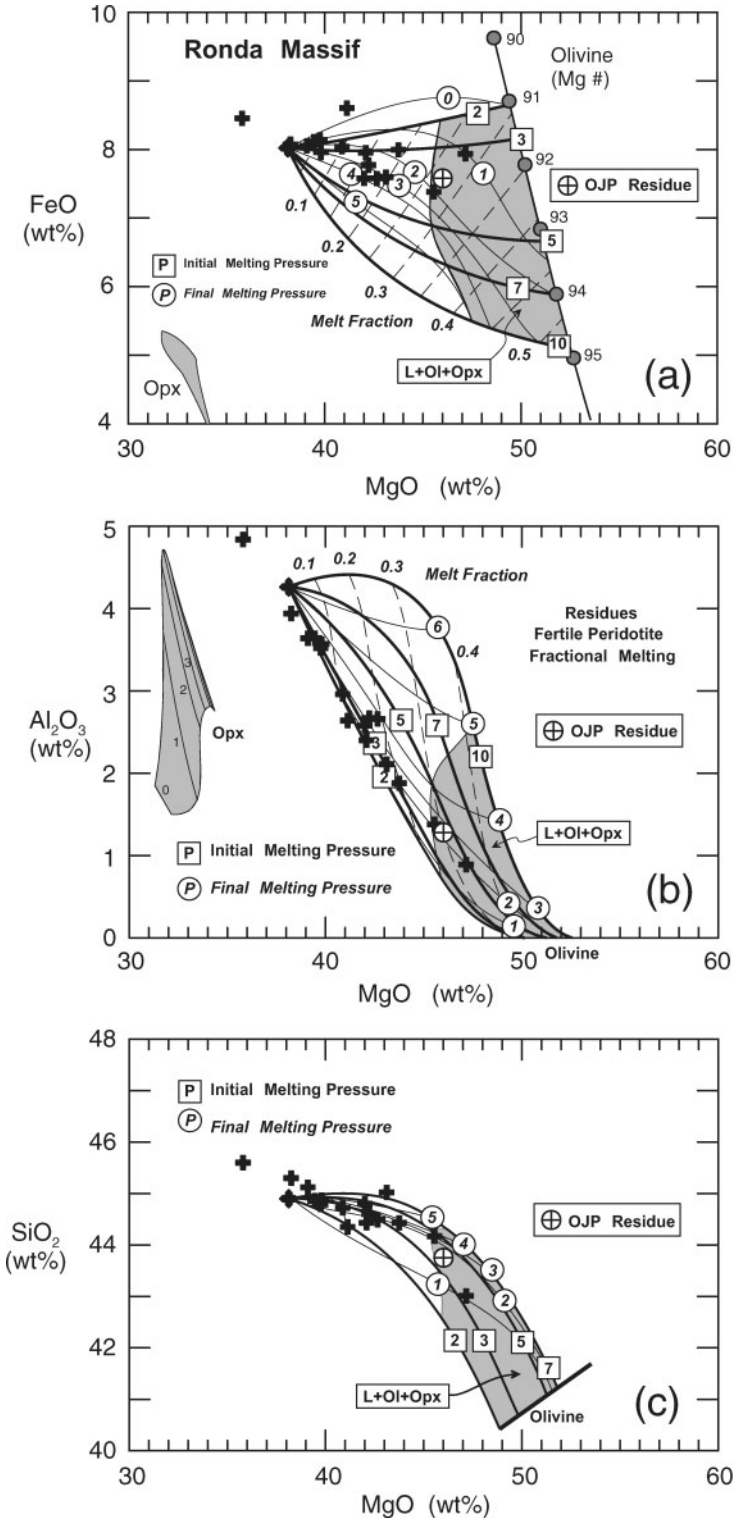

Fig. 4. Ronda peridotite compositions (bold crosses) compared with model residues formed by fractional melting of fertile peridotite KR-4003. Bold lines labelled with squares, initial melting pressures; light lines labelled with circles, final melting pressures; light dashed lines, melt fractions; gray shaded fields, compositions of residual harzburgite designated as [L + Ol + Opx].

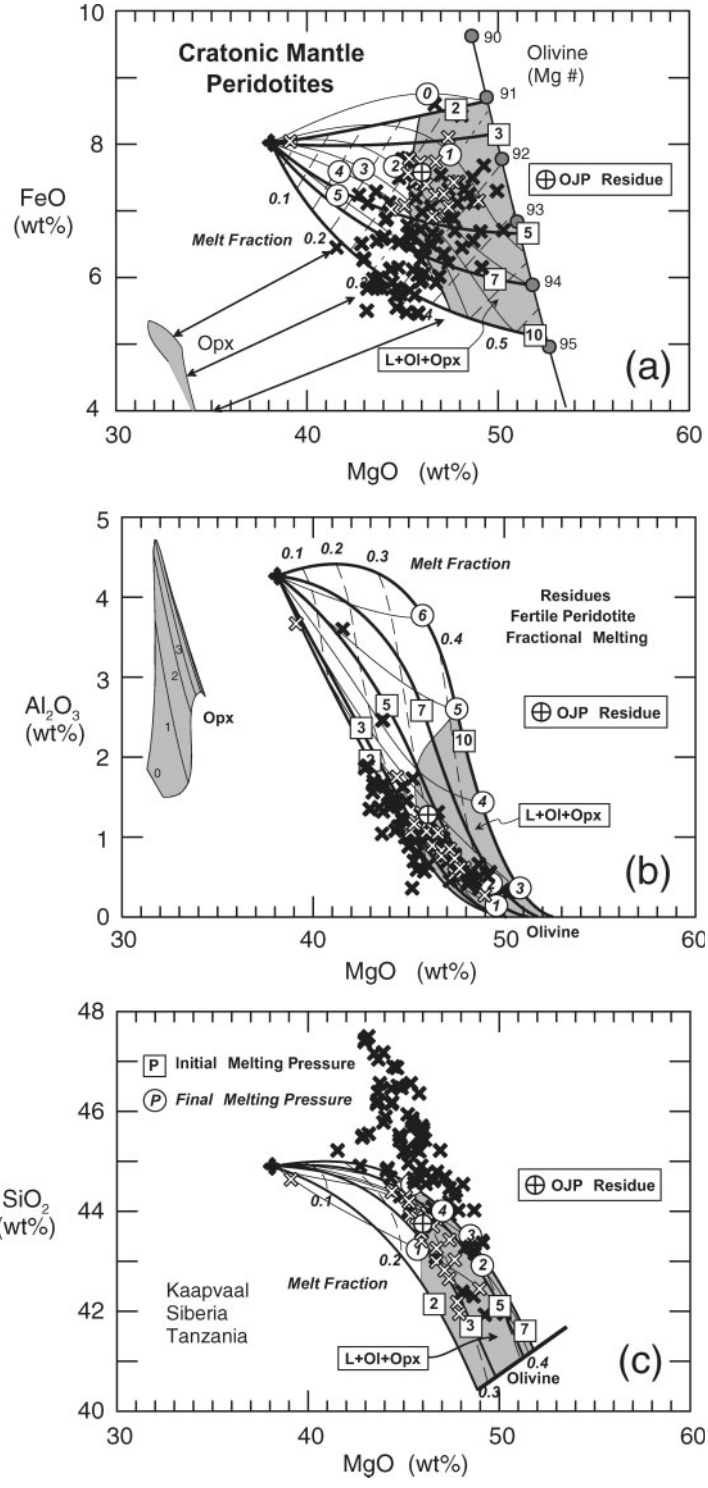

Fig. 5. Cratonic peridotite compositions compared with model residues formed by fractional melting of fertile peridotite KR-4003. Bold lines labelled with squares, initial melting pressures; light lines labelled with circles, final melting pressures; light dashed lines, melt fractions; gray shaded fields, compositions of residual harzburgite designated as [L + Ol + Opx]. The three lines terminated with arrows and stemming from Opx define *mg*-numbers of 92, 93, and 94. Open cross symbols are potential residues with internally consistent initial melting pressures and melt fractions in combined $MgO–SiO_2$, $MgO–Al_2O_3$, and MgO–FeO space. These plot in the field defined by harzburgite residues, in good agreement with petrographic observations (e.g. Boyd *et al.*, 1993, 1997, 1999). Closed cross symbols are orthopyroxene-rich samples that display inconsistent melting pressures and melt fractions in combined $MgO–SiO_2$, $MgO–Al_2O_3$, and MgO–FeO space. Opx-poor and -rich xenoliths are predicted to contain olivines with *mg*-numbers in the 92–94 range, in excellent agreement with observations (e.g. Boyd *et al.*, 1993, 1997, 1999). OJP is a model residue computed by mass balance from the model primary magma from the Ontong Java Plateau (Herzberg, 2004*a*).

exhibit initial melting pressures at about 2 GPa, similar to abyssal peridotites.

Hot Ronda residues are similar to a model residue composition for the Ontong Java Plateau, computed by mass balance from the calculated primary fractional melt composition presented by Herzberg (2004*a*). The Ontong Java Plateau is a region of thickened crust that might have formed by melting in a Cretaceous plume (Neal *et al.*, 1997; Fitton & Godard, 2004). The initial source is very similar in composition to fertile peridotite KR-4003 (Herzberg, 2004*a*). A model residue for Hawaii would be equally desirable, but there is some indication that the initial source is not similar to KR-4003 (Herzberg & O'Hara, 2002; Feigenson *et al.*, 2003). Even more desirable would be xenoliths of residues from the active Hawaiian plume. However, xenoliths from Hawaii (Sen, 1987) are more likely to be magmatic cumulates, and lherzolite xenoliths from Oahu are probably pieces of the lithosphere (Yang *et al.*, 1998). The Ontong Java Plateau example is used throughout this paper as a reference model residue formed by fractional melting of a fertile peridotite in a modern plume situation.

The results presented here are in good agreement with the suggestion of Frey *et al.* (1985) that the Ronda peridotite massif is a fossil plume or mantle diapir. Residues with the highest MgO contents may have been located in the hot core of the plume where melting initiated at the highest pressures. Conversely, residues with the lowest MgO contents may have been located at the periphery or diapir–wall rock interface (Frey *et al.*, 1985) where the initial melting pressure and extent of melting were both at a minimum.

Peridotite xenoliths from the Kaapvaal, Siberian and Tanzanian cratons

Kimberlite-hosted peridotite xenoliths from the Kaapvaal, Siberian and Tanzanian cratons have Re–Os model ages that range from Proterozoic to Archean, with the majority being Archean (Pearson *et al.*, 1995; Carlson *et al.*, 1999; Chesley *et al.*, 1999). Of the low- and high-temperature equilibrated xenoliths, only the low-temperature types are considered here because metasomatism is extensive in the high-temperature types (e.g. Smith & Boyd, 1987; Griffin *et al.*, 1989). Xenolith compositions plotted in Fig. 5 (Boyd & Mertzman, 1987; Boyd *et al.*, 1993, 1997, 1999; Lee & Rudnick, 1999) have been divided into two populations. The first consists of peridotites that display the properties of residues produced by initial melting at 3–5 GPa in combined MgO–SiO_2, MgO–Al_2O_3, and MgO–FeO space (Fig. 5a–c; open cross symbols). All others are too enriched in orthopyroxene to be residues (Fig. 5a–c; filled cross symbols), a conclusion reached previously (Kelemen *et al.*, 1992, 1998; Herzberg, 1993, 1999; Smith *et al.*, 1999). Addition of orthopyroxene will create a whole rock with high apparent initial melting pressures when viewed in MgO–FeO (Fig. 5a) and MgO–SiO_2 (Fig. 5c) space, but impossibly low pressures when viewed in Al_2O_3–MgO space (Fig. 5b). Xenoliths that exhibit contradictory pressures cannot be simple residues. These results are consistent with low vanadium contents, which point to Opx enrichment by either melt–rock reaction or cumulus addition (Lee *et al.*, 2003). Peridotite xenoliths from the Slave Craton (Kopylova & Russell, 2000) also display variable orthopyroxene enrichment, and have not been plotted to preserve clarity. Peridotites from Somerset Island (Schmidberger & Francis, 2001) are discussed as a separate issue in Electronic Appendix 3 (http:www.petrology.oupjournals.org).

Orthopyroxene-poor xenoliths from cratonic mantle could have been produced at initial melting pressures of 3–5 GPa and potential temperatures of about 1450–1600°C. Most cratonic peridotites plot in the compositional space defined by harzburgite residues in Fig. 5, in agreement with petrographic observations; the small amounts of garnet and clinopyroxene observed in these samples have been interpreted to be of exsolution or metasomatic origin (Cox *et al.*, 1987; Boyd *et al.*, 1997). These are hot residues, similar to those for Ronda and the Ontong Java Plateau. Similar pressures of initial melting indicate similar potential temperatures for melt extraction (Fig. 2) in geodynamic settings that range from the Archean to the Cretaceous. Some harzburgite xenoliths differ in displaying higher MgO and higher melt fractions compared with Ronda and the Ontong Java Plateau, but dunite is a rare lithology. Reference to Fig. 5 shows that residues with elevated MgO contents can be produced by lower pressures of final melting, indicating the possible involvement of thinner lithosphere in the Archean at the time of melt extraction.

Peridotites from active subduction zones

Peridotites from active subduction zones have been described from the Itinome-gata back-arc in Japan (Kuno & Aoki, 1970; Aoki & Shiba, 1973), the Cascade back-arc (Brandon & Draper, 1996), the Patagonian back-arc (Laurora *et al.*, 2001), the Luzon arc (Maury *et al.*, 1992), the South Sandwich forearc (Pearce *et al.*, 2000), the Izu–Bonin–Mariana forearc (Parkinson & Pearce, 1998), and the Papua New Guinea forearc (McInnes *et al.*, 2001). Whole-rock geochemical data are summarized in Fig. 6. Most arc peridotites have low Al_2O_3 and are more orthopyroxene-rich than residues of fertile mantle peridotite. Similarly, many arc peridotites are enriched in SiO_2 (Fig. 6c), similar to many cratonic mantle samples (Fig. 5c). Some are enriched in FeO_T compared with cratonic mantle, a difference that is discussed below.

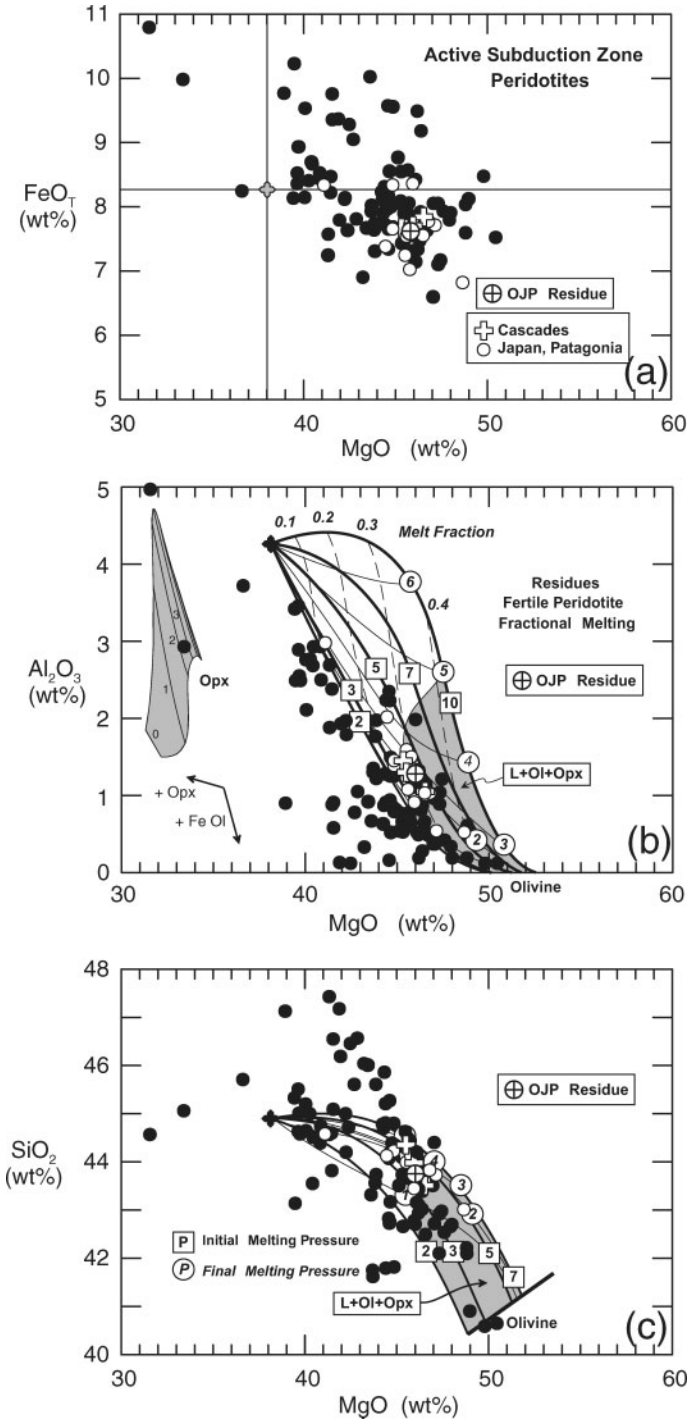

Fig. 6. Peridotites from active subduction zones (Kuno & Aoki, 1970; Aoki & Shiba, 1973; Maury *et al.*, 1992; Brandon & Draper, 1996; Parkinson & Pearce, 1998; Pearce *et al.*, 2000; Laurora *et al.*, 2001; McInnes *et al.*, 2001). Bold lines labelled with squares, initial melting pressures; light lines labelled with circles, final melting pressures; light dashed lines, melt fractions; gray shaded fields, compositions of residual harzburgite designated as [L + Ol + Opx]. No melting grid is given in (a), which displays FeO_T rather than FeO (see text for details). FeO_T is for fertile peridotite KR-4003 (8·02% FeO and 0·29% Fe_2O_3). Addition of Opx and olivine to residues with *mg*-number $<\sim$90 is indicated by vectors in (b). Open symbols are potential residues with internally consistent initial melting pressures and melt fractions in combined MgO–SiO_2, MgO–Al_2O_3, and MgO–FeO space. Closed symbols are orthopyroxene-rich samples that display inconsistent melting pressures and melt fractions in combined MgO–SiO_2, MgO–Al_2O_3, and MgO–FeO space. Most samples are too rich in SiO_2 and too poor in Al_2O_3 to be residues of fertile peridotite. Important exceptions are several xenoliths from back-arc occurrences in Japan, the Cascades, and Patagonia. OJP is a model residue computed by mass balance from the model primary magma from the Ontong Java Plateau (Herzberg, 2004*a*).

Peridotites from active subduction zones contain pyroxenes and spinels with high Fe^{3+}, indicative of elevated oxygen fugacities (Wood *et al.*, 1990; Brandon & Draper, 1996; Parkinson & Pearce, 1998; Parkinson & Arculus, 1999; Pearce *et al.*, 2000). However, vanadium contents reveal a more reducing oxygen fugacity (Canil, 2002; Lee *et al.*, 2003). It has been suggested that vanadium is recording the oxygen fugacity of the residue protolith, and Fe^{3+} is a record of subsequent melt–rock reaction (Lee *et al.*, 2003). Elevated oxygen fugacity during melt–rock reaction will increase the content of Fe_2O_3 in arc peridotites relative to those computed with equation (1); accordingly, only total iron contents (i.e. FeO_T) are given in Fig. 6a. Some arc peridotites are low in FeO_T, comparable with hot residues. Others are unusually iron-rich, probably owing to addition of Fe^{3+} from melts or hydrous fluids from the subducting slab (Lécuyer & Ricard, 1999; Parkinson & Arculus, 1999). This oxidized metasomatic component might add SiO_2 that reacts with peridotite in the mantle wedge to produce orthopyroxene.

Although oxygen fugacities are highly elevated in peridotites from the back-arc occurrences of Itinome-gata and the Cascades (Brandon & Draper, 1996; Parkinson & Arculus, 1999), Fe_2O_3 might be lower compared with arc locations owing to reduced slab fluid or melt fluxes behind the volcanic front. Indeed, a few peridotites from back-arc occurrences in Japan, the Cascades, and Patagonia are very similar to hot peridotite residues (Fig. 6b and c). These are the only reported peridotites from active subduction zones that display internally consistent melting pressures and melt fractions when viewed in combined $MgO–SiO_2$, $MgO–Al_2O_3$, and MgO–FeO space, and they also have the lowest FeO_T. Indeed, xenoliths from Patagonia (Laurora *et al.*, 2001) are located about 400 km from the Chile trench and show the least enrichment in SiO_2 and FeO_T. Clearly, some peridotites from back-arc regions have survived the effects of melt–rock reaction.

Peridotites from subduction zones that have the lowest FeO_T and highest *mg*-numbers might be characteristic of first-stage residues before they become affected by melt–rock interaction. As first-stage residues from subduction zones are similar in composition to hot residues expected in plumes, they might have formed in buoyant oceanic plateaux. Niu *et al.* (2003) examined this possibility, and they concluded that subduction might be initiated at locations where there is a change from ridge-type to plateau-type oceanic lithospheric mantle. Oceanic plateaux might become buoyant platforms on which new continental crust can accrete (e.g. Jordan, 1978, 1988; Ben-Avraham *et al.*, 1981; Abbott & Mooney, 1995; Albarède, 1998; Herzberg, 1999; Niu *et al.*, 2003). The petrology of arc peridotite residues reported here provides strong support for this class of model. However, buoyant residues might also have been produced in hot ridge type environments during the Archean, an alternate possibility that is examined below.

Silica-rich mantle peridotites from active subduction zones and cratonic mantle

Many peridotites from active subduction zones and cratonic mantle are very similar in displaying orthopyroxene enrichment relative to hot residues (Figs 5 and 6). This is displayed by similar systematics in $MgO–SiO_2$ and $MgO–Al_2O_3$ space. There is, however, an important difference as shown in Fig. 7. Opx-rich cratonic mantle tends to be low in FeO_T (Fig. 5a). In contrast, some Opx-rich subduction zone peridotites are rich in FeO_T (i.e. Itinome-gata), whereas others are not (i.e. Luzon arc, Patagonia back-arc).

Orthopyroxene-rich cratonic mantle has been interpreted as a mixture of residues and cumulus orthopyroxene (Herzberg, 1993, 1999), and as a reaction product of residues with a silica-rich melt (Kelemen *et al.*, 1992, 1998; Simon *et al.*, 2003). These two processes cannot be distinguished in plots of $MgO–Al_2O_3$ and $MgO–SiO_2$, but they might produce very different $MgO–FeO_T$ systematics. Kelemen *et al.* (1998) proposed that SiO_2 was added to cratonic mantle residues by partial melts of subducted eclogitic basalt and sediment. Recent progress in numerical simulations indicates that elevated *mg*-number in peridotite might be a possible consequence of the interaction of a basaltic melt with a first-stage residue (Bedini *et al.*, 2003). A melt–rock reaction model is also a suitable explanation for many of forearc peridotites; however, silica might have been added as an oxidized Fe_2O_3 solute-rich hydrous fluid rather than a melt (Parkinson & Pearce, 1998; Parkinson & Arculus, 1999). Melt–rock reaction models for cratonic and subduction zone mantle must, therefore, differ in terms of the melt or fluid compositions that originate from the slab and mantle wedge; these differences have not yet been explored in forward numerical simulations. If progress cannot be made in simulating the formation of FeO-depleted and Opx-rich cratonic mantle by melt–rock reaction, then alternative models must be preferred (e.g. Herzberg, 1993; Francis, 2003).

Peridotites from Tethyan ophiolites

Plotted in Fig. 8 are peridotite compositions from ophiolites in Greece, Cyprus, and Oman (Menzies & Allen, 1974; Lippard *et al.*, 1986; Godard *et al.*, 2000; Takazawa *et al.*, 2003). Many ophiolitic peridotites differ from abyssal peridotites in being depleted in Al_2O_3 and enriched in SiO_2. They are similar to peridotites from subduction zones; however, SiO_2 enrichments are not as extreme. Peridotites in ophiolite sections cannot, therefore, be

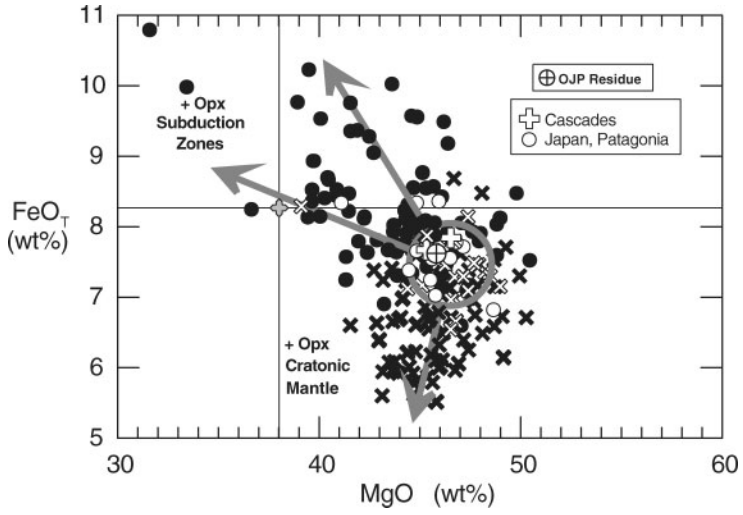

Fig. 7. A comparison of MgO and FeO_T compositions of peridotites from active subduction zones and Archean cratonic mantle. Open symbols are model residues. Closed symbols are too Opx-rich to be residues. (See captions to Figs 5 and 6 for detailed explanation of symbols.) Common compositions enclosed by the gray circle are similar to residues produced by initial melting at 3–5 GPa (Figs 5 and 6). Samples that are enriched in Opx and SiO_2 compared with residues have divergent FeO_T compositions.

single-stage residues of fertile peridotite. They also cannot be second-stage residues of a depleted mantle source as shown in Electronic Appendix 4 (http:www.petrology.oupjournals.org). These results favor models of Tethyan ophiolite formation in back-arc basins and subduction zones rather than open oceans (e.g. Robertson, 2002).

ARCHEAN KOMATIITES AND THEIR RESIDUES

Aluminum-undepleted komatiites

CaO and Al_2O_3 can be fractionated from each other in komatiites that had augite and garnet in the residue. This is likely to be important for understanding the origin of high CaO/Al_2O_3 in aluminum-depleted komatiites, as discussed below. However, fractionation is not significant when melting occurs with residual harzburgite or dunite (e.g. Herzberg & O'Hara, 2002). Therefore, CaO/Al_2O_3 values for liquids and coexisting harzburgite [L + Ol + Opx] or dunite [L + Ol] residues should be similar to that of the peridotite source, as indicated in Fig. 9. Aluminum-undepleted komatiites have CaO/Al_2O_3 ~1·0 (e.g. Nesbitt *et al.*, 1979) as also shown in Fig. 1, similar to fertile mantle peridotite and its depleted residues (Herzberg, 1993; McDonough & Sun, 1995), but considerable scatter is evident for altered samples with low Al_2O_3 owing to Ca mobility (e.g. Herzberg, 1992). Consequently, if we consider this parameter alone, the residue of aluminum-undepleted komatiites could be either harzburgite (Nisbet *et al.*, 1977; Nesbitt *et al.*, 1979; Herzberg & O'Hara, 1998) or dunite (Herzberg & O'Hara, 1998; Sproule *et al.*, 2002). To distinguish between these possibilities, an examination is made of FeO_T and MgO contents of komatiites.

Shown in Fig. 10 are FeO_T and MgO contents of ~2700 Ma aluminum-undepleted komatiites from Belingwe (Zimbabwe), Kambalda (Australia), Alexo and Pyke Hill (Canada) (Bickle *et al.*, 1975, 1993; Arndt *et al.*, 1977; Nisbet *et al.*, 1977, 1987; Arndt, 1986; Lesher & Arndt, 1995; Lahaye & Arndt, 1996; M. Shore, personal communication, 2004). Olivine was incrementally added to and subtracted from representative sample Z5 from Belingwe (Bickle *et al.*, 1993) using a procedure described in the caption to Fig. 10. Compositions of liquids are shown as the gray and black trajectories, and these are connected to coexisting olivine compositions. The coherent negative sloping trend displayed by aluminum-undepleted komatiites from three continents is coincident with the two trajectories, demonstrating that they can be successfully modeled by olivine fractionation. A parental magma having 28–30% MgO would precipitate olivine with an *mg*-number = 94, similar to the maximum observed *mg*-numbers of olivines in the lava flows (Arndt, 1986; Renner *et al.*, 1994; Lesher & Arndt, 1995). These parental magma compositions are in excellent agreement with previous estimates (Arndt, 1986; Lesher & Arndt, 1995).

To evaluate the residuum mineralogy, the assumption is made that the estimated parental magma compositions shown in Fig. 10 are identical to the primary magma. Primary magmas that exit the melting regime in the mantle must erupt directly to the surface without crystallization for this assumption to be valid. Primary komatiite magmas that enter sills and fractionate olivine

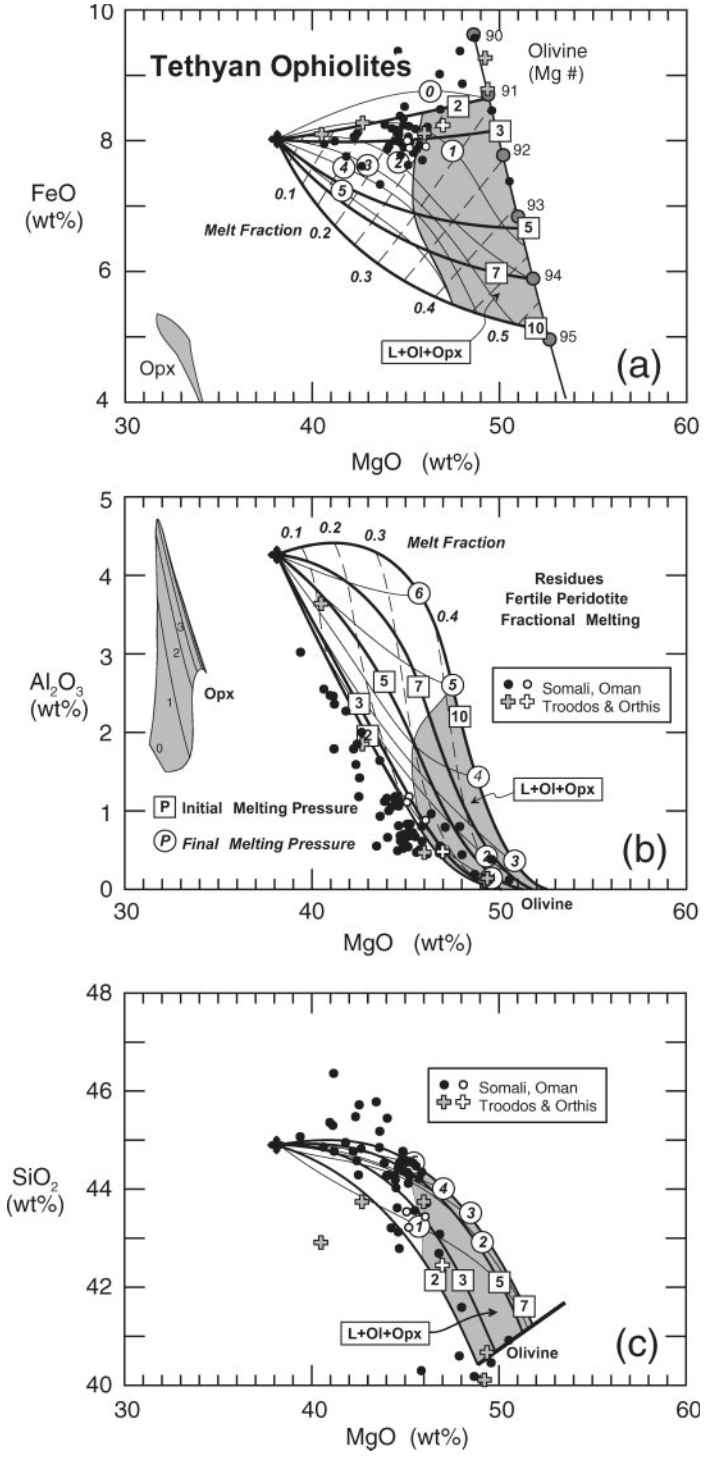

Fig. 8. Peridotites from the mantle sections of Tethyan ophiolites compared with model residues formed by fractional melting of fertile peridotite KR-4003. Bold lines labelled with squares, initial melting pressures; light lines labelled with circles, final melting pressures; light dashed lines, melt fractions; gray shaded fields, compositions of residual harzburgite designated as [L + Ol + Opx]. Open symbols, potential residues with internally consistent initial melting pressures and melt fractions in combined MgO–SiO_2, MgO–Al_2O_3, and MgO–FeO space. Closed symbols, orthopyroxene-rich samples that display inconsistent melting pressures and melt fractions in combined MgO–SiO_2, MgO–Al_2O_3, and MgO–FeO space. Many samples are too rich in SiO_2 and too poor in Al_2O_3 to be residues of fertile peridotite, similar to peridotites from active subduction zones.

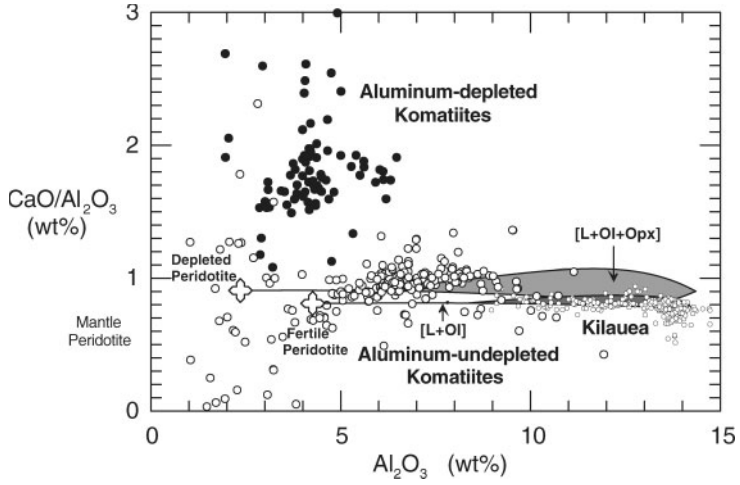

Fig. 9. Ranges of Al_2O_3 and CaO/Al_2O_3 in Archean komatiites compared with liquids produced by equilibrium partial melting of fertile peridotite KR-4003 and depleted abyssal peridotite, from Herzberg & O'Hara (2002). Open crosses, peridotite compositions. Liquid and peridotite compositions are given again in Tables A1 and A3 in Electronic Appendix 1 (http:www.petrology.oupjournals.org). Abyssal peridotite composition is from Baker & Beckett (1999). Gray region labelled [L + Ol + Opx] represents liquids in equilibrium with harzburgite residue. Lines labelled [L + Ol], liquids in equilibrium with olivine. Large filled circles, aluminum-depleted komatiites from the Barberton greenstone belt (Viljoen & Viljoen, 1969; Nesbitt *et al.*, 1979; Smith & Erlank, 1982; Lécuyer *et al.*, 1994). Large open circles, aluminum-undepleted komatiites from Belingwe, Kambalda, Alexo, and Pyke Hill (Bickle *et al.*, 1975, 1993; Arndt *et al.*, 1977; Nisbet *et al.*, 1977, 1987; Arndt, 1986; Lesher & Arndt, 1995; Lahaye & Arndt, 1996; M. Shore, personal communication, 2004). Small open circles, Kilauea lavas [data sources listed by Herzberg & O'Hara (2002)].

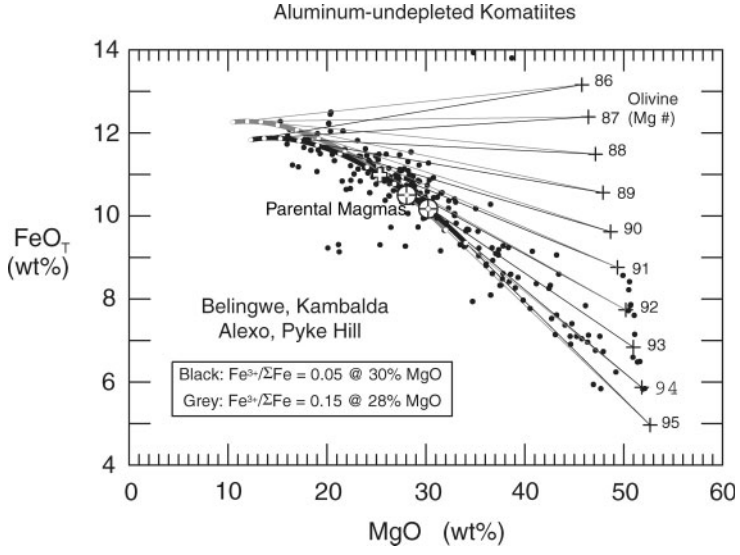

Fig. 10. MgO and FeO_T contents of aluminum-undepleted komatiites compared with magmas and their coexisting equilibrium olivine compositions. Komatiite database is given in the Fig. 9 caption and the text. Olivine was incrementally added to and subtracted from representative sample Z5 from Belingwe shown as the open cross (Bickle *et al.*, 1993; MgO 25·33%, FeO_T 10·98% normalized anhydrous) using Fe–Mg exchange between olivine and liquid (Herzberg & O'Hara, 2002). As Fe_2O_3 does not enter olivine, it was assumed that sample Z5 contained $Fe^{3+}/\Sigma Fe = 0{\cdot}05$ (black trajectory) and 0·15 (gray trajectory). Tie-lines connect liquid compositions in each trajectory with coexisting olivine compositions. Crosses-in-circles, parental magmas that would precipitate olivine with *mg*-number = 94; these contain 28% MgO for $Fe^{3+}/\Sigma Fe = 0{\cdot}15$ and 30% MgO for $Fe^{3+}/\Sigma Fe = 0{\cdot}05$.

will be transformed to derivative liquids with MgO ≤28–30%. A comparison can then be made of these primary magmas with the range of possible FeO_T and MgO contents in primary magmas that form by equilibrium and accumulated fractional melting of an assumed fertile peridotite source, using the computational procedures described by Herzberg & O'Hara (2002). The fertile source composition is that of McDonough & Sun (1995) with FeO_T adjusted to 0·27% Fe_2O_3 and 7·79% FeO using the method of Canil *et al.* (1994). Fe_2O_3 is treated

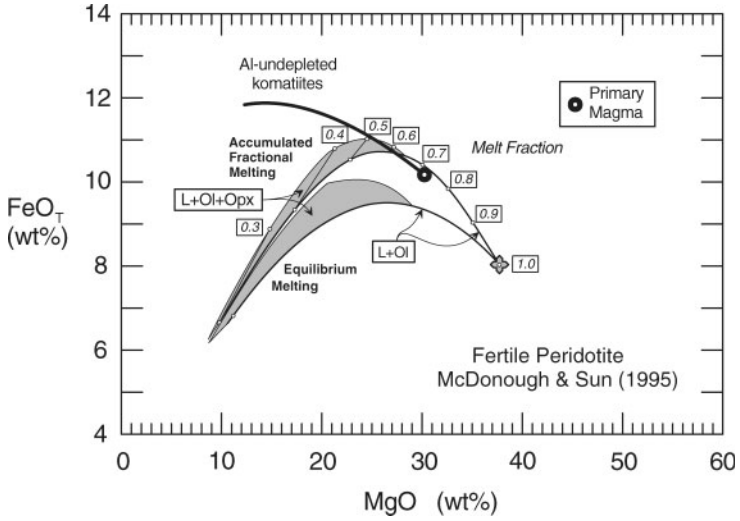

Fig. 11. MgO and FeO_T contents of potential primary magmas produced by equilibrium and accumulated fractional melting of a fertile peridotite composition (McDonough & Sun, 1995). Gray shaded fields represent compositions of liquids separated from harzburgite and designated as [L + Ol + Opx]. Black trajectory is the range of derivative liquids produced by fractional crystallization of olivine from the primary magma shown, and describes the alumina-undepleted komatiites in Fig. 10.

as totally incompatible in olivine and highly incompatible in orthopyroxene (Herzberg & O'Hara, 2002). Results in Fig. 11 show the full range of possible liquid compositions that can be extracted with olivine and harzburgite as residual assemblages. All liquids produced by equilibrium melting are too low in FeO_T compared with the primary komatiite magma. The match is improved for the case of accumulated fractional melting where olivine is the only residuum phase (Fig. 11). There are, however, several possible difficulties with this model. The melt fraction is about 0·7, which might be excessive. The residuum olivine would have an *mg*-number of 98 (Herzberg & O'Hara, 2002, fig. 7b), and dunites having this composition have never been reported. Dunites are a rare lithology in xenoliths of cratonic mantle and, where reported, the most forsteritic olivines have *mg*-numbers of 93 (Lee & Rudnick, 1999; see Fig. 5a). Komatiites are rare in comparison with basalts in Archean greenstone belts, and it is reasonable to expect that residuum dunites would be even more rare, given that they resided in the mantle; they may also have been subjected to modification by iron-rich magmas in the mantle. Alternatively, dunites having *mg*-numbers of 98 may not be observed because fractional melting of fertile peridotite may be an inappropriate model.

Another model is shown in Fig. 12 for a depleted peridotite composition. The abyssal peridotite source used in Fig. 9 was found to be too depleted to provide any liquid composition that could match the komatiite primary magma. However, successful solutions were found, by trial and error, using a slightly less depleted source having 41·0% MgO, 7·8% FeO, and 0·27% Fe_2O_3. Total iron contents of depleted and fertile source compositions can be very similar despite the large variations in Al_2O_3 as shown in Fig. 3 for abyssal peridotite. The major element geochemistry of such a source is similar to a residue produced by about 10% basaltic melt extraction from a McDonough & Sun (1995) fertile peridotite. A depleted source is required from observed light rare earth element (LREE) and isotopic depletions (Arndt, 1986; Bickle *et al.*, 1993; Chauvel *et al.*, 1993; Lesher & Arndt, 1995; Lahaye & Arndt, 1996). Inspection of Fig. 12 shows that the primary komatiite magma is similar to a liquid that could have formed by 0·5 mass fractions of equilibrium melting. Accumulated fractional melting is not a possible model solution because it would form liquids with FeO_T contents higher than that of the komatiite primary magma. The residue would have been pure dunite with an *mg*-number of 94; harzburgite is not an acceptible residue. Olivines approaching *mg*-numbers of 94 have been reported for cratonic mantle xenoliths (Boyd *et al.*, 1997; Lee & Rudnick, 1999). However, these are rare and they occur in harzburgites rather than dunites. The lack of dunite residues of aluminum-undepleted komatiites with *mg*-numbers of either 94 or 98 does not permit a determination to be made about whether melting was equilibrium or fractional.

Aluminum-depleted komatiites

As noted above, aluminum-depleted komatiites are characterized by much higher CaO/Al_2O_3 ratios than aluminum-undepleted komatiites (Fig. 9). High ratios must reflect the source composition when olivine and harzburgite are residues because CaO and Al_2O_3 fractionation is not significant (e.g. Herzberg & O'Hara, 2002).

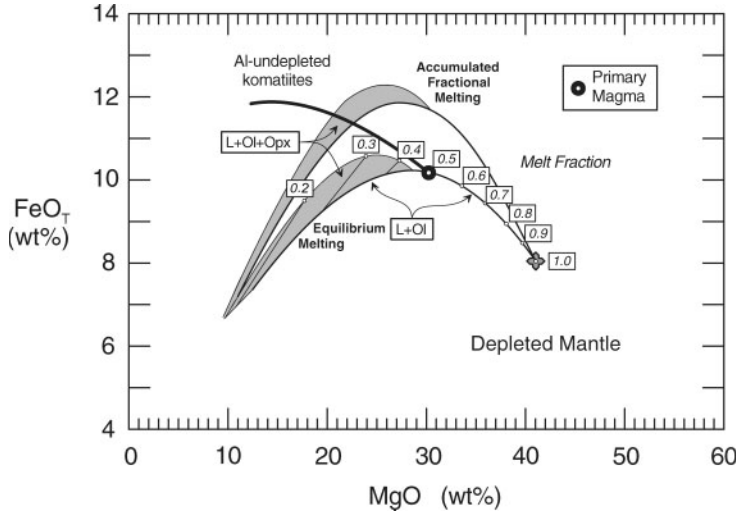

Fig. 12. MgO and FeO_T contents of potential primary magmas produced by equilibrium and accumulated fractional melting of a depleted peridotite composition given in the text. Gray shaded fields represent compositions of liquids separated from harzburgite and designated as [L + Ol + Opx]. Black trajectory is the range of derivative liquids produced by fractional crystallization of olivine from the primary magma shown, and describes the alumina-undepleted komatiites in Fig. 10.

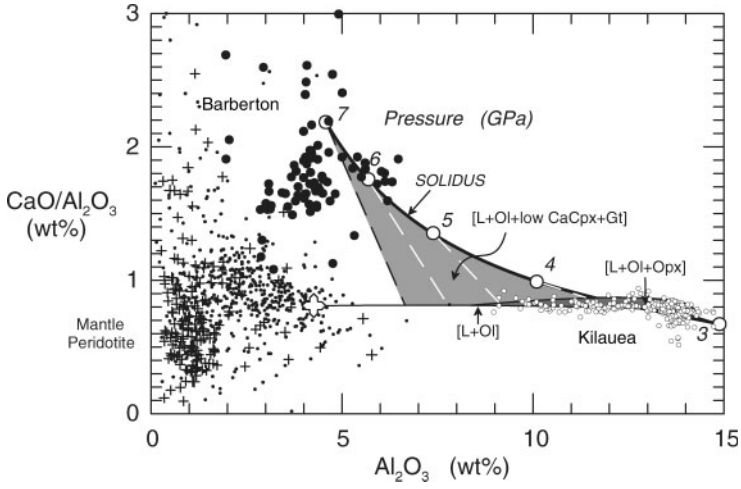

Fig. 13. Variations of Al_2O_3 vs CaO/Al_2O_3 of liquids produced by equilibrium partial melting of fertile peridotite KR-4003 from Walter (1998) and Herzberg & O'Hara (2002). Liquids on the solidus were determined by linear extrapolations of Walter (1998) data to $F = 0$. Liquids for [L + Ol] and [L + Ol + Opx] were reported by Herzberg & O'Hara (2002), and are given again in Electronic Appendix 1 (http:www.petrology.oupjournals.org). Open cross, peridotite KR-4003. Shaded field containing dashed lines represents liquids in equilibrium with olivine + low-Ca clinopyroxene + garnet [L + Ol + low CaCpx + Gt] at the pressures of the isobaric cotectics shown; experiments and modeling indicate that this assemblage is stable for melt fractions in the 0–0·50 range at 7 GPa (Herzberg & O'Hara, 2002). This crystalline assemblage is likely to transform in the subsolidus to an assemblage of garnet harzburgite with minor augite. Large filled circles, Barberton komatiites (Viljoen & Viljoen, 1969; Nesbitt *et al.*, 1979; Smith & Erlank, 1982; Lécuyer *et al.*, 1994). Small open circles, Kilauea lavas (Herzberg & O'Hara, 2002). Dots, Proterozoic mantle peridotites (Herzberg, 1993). Crosses, Archean peridotite xenoliths from the Kaapvaal, Siberian, Tanzanian, and North American cratons (Boyd & Mertzman, 1987; Boyd *et al.*, 1993, 1997, 1999; Lee & Rudnick, 1999; Kopylova & Russell, 2000; Schmidberger & Francis, 2001), and East Greenland (Hanghøj *et al.*, 2001).

Parman *et al.* (1997) and Grove *et al.* (1999) have proposed that aluminum-depleted Barberton komatiites with $CaO/Al_2O_3 \cong 1{\cdot}8$ were generated by hydrous partial melting leaving a harzburgite residuum. This residue must also have $CaO/Al_2O_3 \cong 1{\cdot}8$ and this value must be similar to that of the source, which is considerably higher than 0·8 for fertile peridotite (McDonough & Sun, 1995) and 0·9 for average depleted mantle peridotite (Herzberg, 1993). This model requires an unusual source composition that is not observed in fertile peridotites (Fig. 13). The few peridotites with CaO/Al_2O_3 that are comparable with Barberton komatiites are also

exceptionally depleted in Al_2O_3, and cannot be a plausible initial source. Additionally, depletions in heavy rare earth elements (HREE) exhibited by Barberton komatiites are a feature of a garnet-bearing residue rather than harzburgite (Sun & Nesbitt, 1978; Nesbitt *et al.*, 1979). Other difficulties with this model have been discussed elsewhere (Arndt *et al.*, 1998; Arndt, 2003).

Barberton alumina-depleted komatiites are similar in composition to experimental anhydrous liquids in equilibrium with olivine, subcalcic clinopyroxene, and garnet [i.e. L + Ol + low-Ca Cpx + Gt] produced in excess of 7 GPa (Fig. 13; Herzberg, 1992; Walter, 1998). For an assumed anhydrous fertile peridotite source (McDonough & Sun, 1995), aluminum-depleted komatiites with elevated CaO/Al_2O_3 shown in Fig. 13 must be mass-balanced with residua having low CaO/Al_2O_3 (i.e. olivine + subcalcic clinopyroxene + garnet; Herzberg, 1992; Walter, 1998). Residual garnet is consistent with the REE characteristics of Al-depleted komatiites that show depletions in the HREE. Residues of aluminum-depleted komatiites have not been reported, and this might again reflect the general rarity of komatiites in Archean greenstone belts.

Archean komatiite residues and cratonic lithospheric mantle: a misconnection

There is a rough complementarity between the major element geochemistry of Archean komatiites and cratonic lithospheric mantle xenoliths, an observation that has led many workers to propose a genetic link (O'Hara *et al.*, 1975; Maaloe & Aoki, 1977; Hanson & Langmuir, 1978; Takahashi, 1990; Canil, 1992; Herzberg, 1993, 1999; Walter, 1998). In particular, cratonic lithospheric mantle is highly depleted in incompatible elements, consistent with it being a residue from high degrees of partial melting. However, with the exception of Herzberg (1999), none of the above workers provided quantitative mass balance calculations with respect to any particular mantle source. Herzberg (1999) noted that equilibrium melting of fertile peridotite produces melts with FeO contents lower than those of Al-undepleted komatiites, a misfit that is reproduced in this study (Fig. 11). The suggestion that this misfit might be explained by some form of fractional melting (Herzberg, 1999) appears to hold (Fig. 11). However, this model might be problematic because it predicts olivines in the residue with an *mg*-number of 98 (see Herzberg & O'Hara, 2002), and these have never been observed.

Samples of low temperature-equilibrated Archean cratonic mantle are mostly harzburgites with lesser lherzolites (Nixon & Boyd, 1973; Boyd & Mertzman, 1987; Boyd *et al.*, 1993, 1997, 1999; Lee & Rudnick, 1999; Kopylova & Russell, 2000; Hanghøj *et al.*, 2001; Schmidberger & Francis, 2001). Petrographic descriptions provided by these researchers are in good agreement with whole-rock data that plot in the compositional fields defined by harzburgite and lherzolite, not dunite (Fig. 5). The few cases of dunite that have been reported are shown in Fig. 5, and these have olivines with *mg*-numbers that are typically <93 (Lee & Rudnick, 1999). In contrast, the inferred residue of aluminum-undepleted komatiite is dunite with *mg*-numbers of 94 and 98 for equilibrium and fractional melting models, respectively. The inferred residue of aluminum-depleted komatiite is an unusual assemblage of Ol + low-Ca Px + Gt, which is expected to re-equilibrate in the subsolidus to garnet harzburgite with minor clinopyroxene. Residues of aluminum-depleted and -undepleted komatiites have never been observed as xenoliths of cratonic mantle peridotite. It is concluded, therefore, that cratonic lithospheric mantle did not form as a residue from Archean komatiite melt extraction. How then do we explain its geochemistry? One way to explore this problem is to seek alternatives to Al-depleted and -undepleted komatiites. This is examined in the next section.

INFERRING PRIMARY MAGMA COMPOSITIONS FROM MANTLE PERIDOTITES

Estimates have been made of primary magma compositions for modern MORB and Phanerozoic plume lavas produced by accumulated fractional melting of fertile and depleted sources (Herzberg & O'Hara, 2002; Herzberg, 2004*a*, 2004*b*). Results displayed in Fig. 14a show that there is a simple and linear relationship between MgO and FeO_T, and this can be described by the equation

$$FeO_T = 1{\cdot}933 + 0{\cdot}489MgO. \quad (2)$$

It is useful to compare these primary magma compositions for lavas with those that can be inferred from peridotite residues. An aggregate fractional melt is not in equilibrium with its residue. Only the final drop of liquid extracted is in equilibrium with the residue. However, mass balance must be determined with the standard equation

$$C_o = FC_L + (1-F)C_S \quad (3)$$

where C_o is the initial source composition, F is the mass fraction of the aggregate melt, C_L is the aggregate liquid composition, and C_S is the composition of the residue in equilibrium with the last drop of liquid extracted. The aggregate fractional melt composition can be computed for Opx-poor cratonic mantle, Ronda peridotite, and abyssal peridotite using equation (3) and the following initial source compositions for fertile peridotite KR-4003:

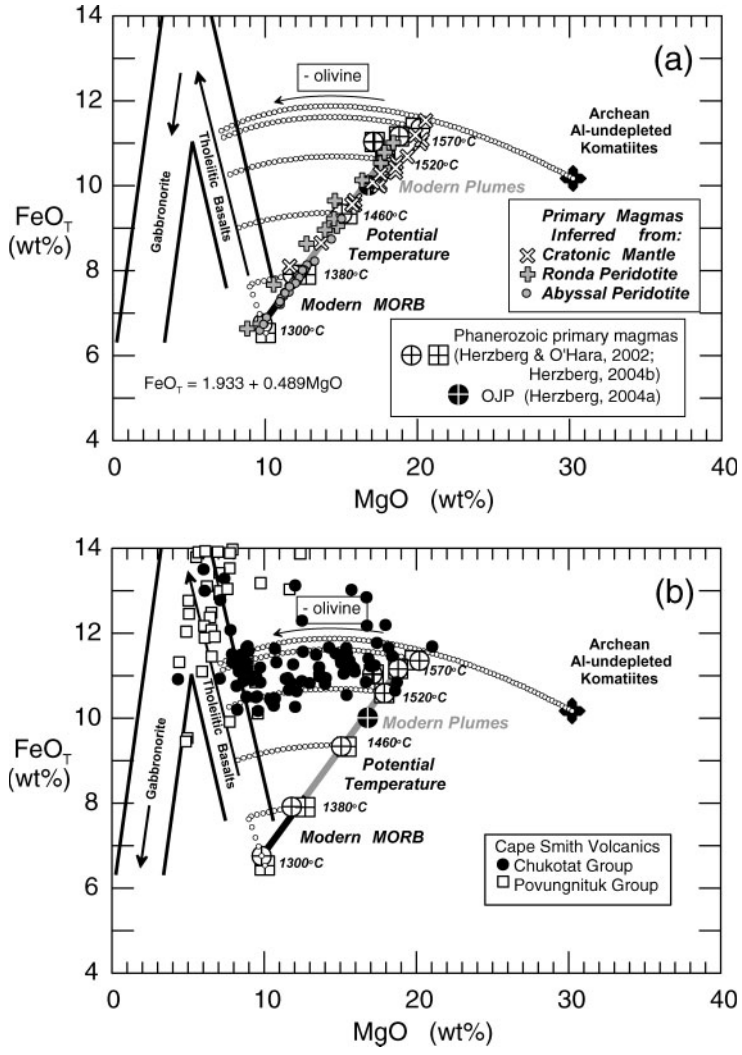

Fig. 14. Summary of MgO and FeO_T for primary magmas. (a) Phanerozoic primary magmas shown as crosses-in-circles and crosses-in-squares have been estimated for eruptives with only olivine as a phenocryst phase, and for accumulated fractional melting of fertile and depleted peridotite compositions, respectively; these can be described by the equation $FeO_T = 1{\cdot}933 + 0{\cdot}489MgO$. Primary magmas are inferred from peridotite residues using equation (3) in the text. Inferred primary magmas from abyssal peridotite are based on the whole-rock model of Baker & Beckett (1999). Primary magmas inferred from both peridotite residues and olivine-phyric eruptives are very similar. Potential temperatures for the primary magmas are from Herzberg & O'Hara (2002). Field labelled 'tholeiitic basalts' shows FeO_T enrichment for modern MORB from the East Pacific Rise and Mid-Atlantic Ridge as a result of fractionation of olivine + plagioclase and olivine + plagioclase + augite (MORB database in petdb.ldeo.columbia.edu). Field labelled 'gabbronorite' shows FeO_T depletion as a result of fractionation of plagioclase + augite + low-Ca pyroxene + magnetite (MORB database in petdb.ldeo.columbia.edu). (b) Volcanics from the Cape Smith belt of early Proterozoic age display an olivine control that extends to inferred primary magmas with 18–20% MgO and potential temperatures of 1520–1570°C.

MgO 38·12%, FeO 8·02%, and Fe_2O_3 0·22% for abyssal peridotite or Fe_2O_3 0·29% for all others. These Fe_2O_3 contents yield computed $Fe^{3+}/\Sigma Fe = 0{\cdot}07$–$0{\cdot}10$ in primary magmas from ridge and plume occurrences, similar to those occurring in nature (Herzberg & O'Hara, 2002). Whole-rock data provide C_S in equation (3), and the melt fraction F for each peridotite was obtained directly from Figs 3a, 4a and 5a. Solutions for aggregate liquid compositions are shown in Fig. 14a. These are model primary magmas that formed as aggregate fractional melts, complementary to residues of cratonic mantle, Ronda peridotite, and abyssal peridotite.

Inferred primary magmas that are complementary to abyssal peridotites mostly contain 10–13% MgO, very similar to those that have been estimated for MORB (Herzberg & O'Hara, 2002; Herzberg, 2004*b*; Herzberg *et al.*, submitted). Inferred primary magmas that are complementary to Ronda peridotites contain 9–18% MgO; these are similar to those that have been estimated by Frey *et al.* (1985), and to those from both MORB

and Phanerozoic plumes (Herzberg & O'Hara, 2002; Herzberg *et al.*, submitted). Primary magmas inferred for Archean cratonic mantle generally contain 16–20% MgO and these are also similar to primary magmas from plume associations of Phanerozoic age (Herzberg & O'Hara, 2002; Herzberg, 2004*a*, 2004*b*). Variations in the MgO contents of primary magmas are mostly produced by variations in mantle potential temperature, and those shown in Fig. 14 are from Herzberg & O'Hara (2002). Potential temperatures inferred from cratonic mantle peridotite range from about 1450 to 1600°C, very similar to those from Phanerozoic plume occurrences.

Another important observation is that MgO contents of primary magmas inferred for Archean cratonic peridotite (16–20% MgO) were much lower than 30% MgO for aluminum-undepleted komatiites (Fig. 14a). This is another way of showing that there is no petrogenetic connection between Archean cratonic mantle and aluminum-undepleted komatiites (see above).

If cratonic peridotite is so similar in composition to residues expected from plume occurrences of Phanerozoic age, what does that say about the plume model of cratonic mantle formation (Herzberg, 1993, 1999)? Data for Cape Smith picrites and basalts of early Phanerozoic age (Picard, 1989; Picard *et al.*, 1990; Francis *et al.*, 1983) are also shown in Fig. 14b. Basalts of the Povungnituk Group have MgO and FeO_T contents that are characteristic of fractionated basalts (Fig. 14b), and these have been interpreted as forming in a shallow marine continental rift environment (Hynes & Francis, 1982; Francis *et al.*, 1983; Picard *et al.*, 1990). Olivine-phyric samples of the Chukotat Group are enriched in MgO compared with basalts from the Povungnituk Group (Fig. 14b), and are actually very similar in composition to Kilauea volcanics in all major elements. Figure 14b shows that volcanics from the Chukotat Group define an olivine fractionation trend that extends to picritic primary magmas having 18–20% MgO. These primary magmas are very similar to Phanerozoic plume-related magmas such as Kilauea, Gorgona, and early Tertiary Iceland, and to those that were complementary to cratonic mantle (Fig. 14a and b). Petrographic and geochemical characteristics were used to suggest that the Chukotat volcanics formed during lithosphere rifting and extension, and that they record a change from continental to oceanic environments (Francis *et al.*, 1981, 1983; Hynes & Francis, 1982; Picard, 1989; Picard *et al.*, 1990). If this is correct, then the geodynamic implications are significant. The Cape Smith volcanics might have formed strictly in a hot ridge if extension was not associated with the impact of a plume. It further suggests that some cratonic mantle of Proterozoic and Archean age might be composed of residues that also formed in hot oceanic ridge environments, with mantle potential temperatures that are characteristic of modern plumes (i.e. ~1450–1600°C). This situation might be very different from the Tertiary North Atlantic igneous province, where rifting along the Greenland margin was associated with the eruption of picrites from the Icelandic plume (e.g. Saunders *et al.*, 1997). Indeed, it may be more analogous to the more common situation further to the south where rifting and formation of the Atlantic Ocean occurred without eruption of picrites and komatiites. There may be considerable doubt about a plume origin inferred for picrites and komatiites with early Proterozoic and Archean ages and MgO contents of 16–20%. This is explored further in the next section.

ARCHEAN PRIMARY MAGMAS

The most common of the primary magmas in the Archean contain 16–20% MgO and formed complementary cratonic mantle by fractional melting. These primary magmas might have differentiated to common basalt that characterizes greenstone belts. A small number of cratonic mantle samples may have formed from primary magmas having 12–13% MgO, similar to modern MORB (Fig. 14a). Aluminum-undepleted komatiites crystallized from primary magmas with about 30% MgO. Constraining the MgO content of the primary magma for aluminum-depleted komatiites is more difficult, and will be examined elsewhere.

As aluminum-undepleted komatiites show no evidence for the involvement of significant amounts of magmatic water (Arndt *et al.*, 1998; Sproule *et al.*, 2002; Arndt, 2003), they were probably formed in mantle plumes. Unfortunately, the potential temperature is difficult to constrain. It must have been considerably higher than 1600°C, the liquidus temperature for a magma with 30% MgO, because potential temperatures are always higher than eruption temperatures (e.g. McKenzie & Bickle, 1988). Small rises in potential temperature can result in large increases in the pressure at which the mantle begins to melt as shown by the *T–P* phase diagram for mantle peridotite (Herzberg & Zhang, 1996; Walter, 1998; Herzberg & O'Hara, 2002). The phase equilibria that controlled the compositions of komatiite might have occurred at 5–10 GPa, and initial melting pressures might have been even higher (Sproule *et al.*, 2002). These pressures and corresponding temperatures are much higher than those that characterize Phanerozoic plume magmatism (Herzberg & O'Hara, 2002). They are also conditions where the densities of komatiite and its residual olivine become similar, and this will favor equilibrium melting over fractional melting (Arndt, 2003). The exact pressure of neutral olivine–liquid density is subject to experimental uncertainty, but it is likely to be in excess of 8 GPa (Agee, 1998; Ohtani *et al.*, 1998). At some stage, eruption of dense komatiite magma will probably follow the buoyancy laws of a feather captured in an upwelling

thermal rather than an olivine crystal in a laboratory experiment (Herzberg, 1992), and equilibrium melting might dominate. Fractional melting will gain in importance when the plume rises to higher levels, where magmas become significantly buoyant with respect to their coexisting crystals. It may be no surprise that a primary komatiite magma with 30% MgO can be successfully modeled with both equilibrium and fractional melting (see above). The ways in which phase equilibria and density impose an imprint on the geochemistry of komatiites in deep plumes are likely to be complex, and readers are referred to Arndt (2003) for a discussion of some possibilities.

This paper ends with a conjecture. The potential temperatures that characterize melt production below modern oceanic ridges are about 1300–1400°C, and in plumes they are about 1450–1600°C (Herzberg *et al.*, submitted). Modern plumes can be hotter than ambient mantle below oceanic ridges by about 100–300°C. If the Cape Smith volcanics formed in a hot ridge rather than a plume, then the ambient mantle during the early Proterozoic would have had a potential temperature of about 1500–1600°C (Fig. 14b). This would imply secular Earth cooling of 50–100°C/Ga, which is fully consistent with thermal models (Pollack, 1997). It is then reasonable to conjecture that, based on analogy with modern ridge and plume magmatism, early Proterozoic and Archean plumes might have had potential temperatures in the 1700–1900°C range. These temperatures would have been sufficient to produce deep and extensive melting that characterizes aluminum-undepleted komatiites. Two important populations of Archean primary magmas, one with about 16–20% MgO and the other with 30% MgO, might simply be a record of ridge and plume activity in an early Earth that was hotter than today.

CONCLUSIONS

The petrology of peridotite residues varies according to the geodynamic setting in which fractional melting takes place. Residues formed at high potential temperatures (T_P) and high initial melting pressures (P_o) are characterized by low FeO, high Al_2O_3 and high SiO_2, relative to MgO. Residues formed by high melt fractions and low final melting pressures are universally elevated in MgO. These effects have been calibrated by a parameterization of experimental data for fertile mantle peridotite, and the results have been applied to natural mantle peridotite samples. The following are specific conclusions.

(1) Abyssal peridotites formed at about $P_o = 2$–3 GPa, consistent with $T_P = 1280$–1400°C for MORB. They are relatively cold compared with plume occurrences described by Herzberg & O'Hara (2002).

(2) High-MgO peridotites from the Ronda massif are interpreted to be hot residues of a fossil plume with $P_o = 3$–5 GPa and $T_P = 1450$–1550°C and melt fractions approaching 0·30. They were formed by extraction of a primary magma with about 18% MgO, similar to modern plume occurrences. More fertile peridotites had minimal melt extracted. Variable initial melting pressures and melt fractions exhibited by Ronda peridotites in a confined region record a 250°C potential temperature gradient in a plume axis.

(3) Most peridotites from subduction zones are too enriched in SiO_2 and too depleted in Al_2O_3 to be residues, and were produced by melt–rock reaction of a precursor peridotite protolith. A few peridotite xenoliths from the Japan, Cascades, and Chile–Patagonian back-arcs appear to be precursors that have escaped some of the effects of melt–rock reaction. They are similar to hot residues formed in plumes, in agreement with the suggestion made by Niu *et al.* (2003).

(4) Many peridotites from ophiolites are too enriched in SiO_2 and too depleted in Al_2O_3 to be residues, and bear the imprint of melt–rock reaction in a subduction zone setting.

(5) Many harzburgite xenoliths from cratonic mantle are too enriched in Opx to be residues, and have SiO_2 and Al_2O_3 contents that are similar to peridotites from active subduction zones. However, FeO_T contents are lower, and it remains to be determined whether they can be successfully explained by melt–rock reaction models (e.g. Kelemen *et al.*, 1998; Bedini *et al.*, 2003).

(6) Many xenoliths of cratonic mantle are harzburgites that have the properties of hot residues formed at $P_o = 3$–5 GPa and $T_P = 1450$–1600°C. They are complementary to primary magmas with 16–20% MgO, very similar to primary magmas that have been estimated for the early Tertiary Icelandic plume, Gorgona, Kilauea, and Ontong Java (Herzberg & O'Hara, 2002; Herzberg, 2004*a*). The primary magmas may have crystallized to common basalts in Archean greenstone belts.

(7) Primary magmas of aluminum-undepleted komatiites in the Archean had 28–30% MgO. They left behind dunite residues with *mg*-numbers of 94 and 98 calculated for equilibrium and fractional melting, respectively. Dunites with these compositions have not been reported, possibly reflecting the rarity of komatiites in Archean greenstone belts, or modification by iron-rich magmas in the mantle.

(8) Residues of aluminum-depleted komatiites consist of the assemblage of olivine + low-Ca pyroxene + garnet with low CaO/Al_2O_3, which is expected to have re-equilibrated in the subsolidus to garnet harzburgite with minor clinopyroxene. These residues have also not been reported.

(9) It follows from conclusions (6)–(8) that cratonic mantle was not produced as residues of Archean komatiites.

ACKNOWLEDGEMENTS

Special thanks go to Mike O'Hara for a stimulating 30 year correspondence on the petrology of mantle peridotite. I am very grateful to Nick Arndt, Cin-Ty Lee, Shantanu Keshav, and Marjorie Wilson for thoughtful and careful reviews. This research was partially supported by a grant from the National Science Foundation (EAR-0228592).

SUPPLEMENTARY DATA

Supplementary data for this paper are available on *Journal of Petrology* online.

REFERENCES

Abbott, D. & Mooney, W. (1995). The structure and geochemical evolution of the continental crust: support for the oceanic plateau model of continental growth. *Reviews of Geophysics*, Supplement, 231–242.

Agee, C. B. (1998). Crystal–liquid density inversions in terrestrial and lunar magmas. *Physics of the Earth and Planetary Interiors* **107**, 63–74.

Albarède, F. (1998). The growth of continental crust. *Tectonophysics* **296**, 1–14.

Aoki, K. & Shiba, I. (1973). Pyroxenes from lherzolite inclusions of Itinome-gata, Japan. *Lithos* **6**, 41–51.

Arndt, N. T. (1986). Differentiation of komatiites flows. *Journal of Petrology* **27**, 279–301.

Arndt, N. T. (2003). Komatiites, kimberlites, and boninites. *Journal of Geophysical Research* **108**(ECV 5), 1–11.

Arndt, N. T., Naldrett, A. J. & Pyke, D. R. (1977). Komatiitic and iron-rich tholeiitic lavas of Munro Township, Northeast Ontario. *Journal of Petrology* **18**, 319–369.

Arndt, N., Ginibre, C., Chauvel, C., Albarède, F., Cheadle, M., Herzberg, C., Jenner, G. & Lahaye, Y. (1998). Were komatiites wet? *Geology* **26**, 739–742.

Asimow, P. D. (1999). A model that reconciles major- and trace-element data from abyssal peridotites. *Earth and Planetary Science Letters* **169**, 303–319.

Asimow, P. D., Hirschmann, M. M. & Stolper, E. M. (2001). Calculation of peridotite partial melting from thermodynamic models of minerals and melts, IV. Adiabatic decompression and the composition and mean properties of mid-ocean ridge basalts. *Journal of Petrology* **42**, 963–998.

Baker, M. B. & Beckett, J. R. (1999). The origin of abyssal peridotites: a reinterpretation of constraints based on primary bulk compositions. *Earth and Planetary Science Letters* **171**, 49–61.

Bedini, R. M., Bodinier, J.-L. & Vernières, J. (2003). Numerical simulation of Fe–Mg partitioning during melting and melt–rock interactions in the upper mantle. *Geophysical Research Abstracts* **5**, 13457.

Ben-Avraham, Z., Nur, A., Jones, D. & Cox, A. (1981). Continental accretion: from oceanic plateaus to allochthonous terranes. *Science* **213**, 47–54.

Bickle, M. J., Martin, A. & Nisbet, E. G. (1975). Basaltic and peridotitic komatiites and stromatolites above a basal unconformity in the Belingwe Greenstone Belt, Rhodesia. *Earth and Planetary Science Letters* **27**, 155–162.

Bickle, M. J., Arndt, N. T., Nisbet, E. G., Orpen, J. L., Martin, A., Keays, R. R. & Renner, R. (1993). Geochemistry of the igneous rocks of the Belingwe greenstone belt: alteration, contamination and petrogenesis. In: Bickle, M. J. & Nisbet, E. G. (eds) *The Geology of the Belingwe Greenstone Belt, Zimbabwe*. Rotterdam: Balkema, pp. 175–213.

Boyd, F. R. & Mertzman, S. A. (1987). Composition and structure of the Kaapvaal lithosphere, southern Africa. In: Mysen, B. O. (ed.) *Magmatic Processes: Physicochemical Principles. Geochemical Society Special Publication* **1**, 13–24.

Boyd, F. R., Pearson, D. G., Nixon, P. H. & Mertzman, S. A. (1993). Low-calcium garnet harzburgites from southern Africa: their relations to craton structure and diamond crystallization. *Contributions to Mineralogy and Petrology* **113**, 352–366.

Boyd, F. R., Pokhilenko, N. P., Pearson, D. G., Mertzman, S. A., Sobolev, N.V. & Finger, L. W. (1997). Composition of the Siberian cratonic mantle: evidence from Udachnaya peridotite xenoliths. *Contributions to Mineralogy and Petrology* **128**, 228–246.

Boyd, F. R., Pearson, D. G. & Mertzman, S. A. (1999). Spinel-facies peridotites from the Kaapvaal root. In: Gurney, J. J., Gurney, J. L., Pascoe, M. D. & Richardson, S. H. (eds) *Proceedings of the 7th International Kimberlite Conference*. Cape Town: Red Roof Design, pp. 40–48.

Brandon, A. D. & Draper, D. S. (1996). Constraints on the origin of the oxidation state of mantle overlying subduction zones: an example from Simcoe, Washington, USA. *Geochimica et Cosmochimica Acta* **60**, 1739–1749.

Canil, D. (1992). Orthopyroxene stability along the peridotite solidus and the origin of cratonic lithosphere beneath southern Africa. *Earth and Planetary Science Letters* **111**, 83–95.

Canil, D. (2002). Vanadium in peridotites, mantle redox and tectonic environments: Archean to present. *Earth and Planetary Science Letters* **195**, 75–90.

Canil, D., O'Neill, H. St. C., Pearson, D. G., Rudnick, R. L., McDonough, W. F. & Carswell, D. A. (1994). Ferric iron in peridotites and mantle oxidation states. *Earth and Planetary Science Letters* **123**, 205–220.

Carlson, R. W., Pearson, D. G., Boyd, F. R., Shirey, S. B., Irvine, G., Menzies, A. H. & Gurney, J. J. (1999). Re–Os systematics of lithospheric peridotites: implications for lithosphere formation and preservation. In: Gurney, J. J., Gurney, J. L., Pascoe, M. D. & Richardson, S. H. (eds) *Proceedings of the 7th International Kimberlite Conference*. Cape Town: Red Roof Design, pp. 99–108.

Chauvel, C., Dupré, B. & Arndt, N. T. (1993). Pb and Nd isotopic correlation in Belingwe komatiites and basalts. In: Bickle, M. J. & Nisbet, E. G. (eds) *The Geology of the Belingwe Greenstone Belt, Zimbabwe*. Rotterdam: Balkema, pp. 167–174.

Chesley, J. T., Rudnick, R. L. & Lee, C.-T. (1999). Re–Os systematics of mantle xenoliths from the East Africa Rift: age, structure, and history of the Tanzanian craton. *Geochimica et Cosmochimica Acta* **63**, 1203–1217.

Cox, K. G., Smith, M. R. & Beswetherick, S. (1987). Textural studies of garnet lherzolites: evidence of exsolution origin from high-temperature harzburgites. In: Nixon, P. H. (ed.) *Mantle Xenoliths*. New York: Wiley, pp. 537–550.

Dick, H. J. B. (1989). Abyssal peridotites, very slow spreading ridges and ocean ridge magmatism. In: Saunders, A. D. & Norry, M. J. (eds) *Magmatism in the Ocean Basins. Geological Society, London, Special Publications* **42**, 71–105.

Dick, H. J. B. & Fisher, R. L. (1984). Mineralogical studies of the residues of mantle melting: abyssal and alpine-type peridotites. In: Kornprobst, J. (ed.) *Kimberlites II: the Mantle and Crust–Mantle Relationships*. Amsterdam: Elsevier, pp. 295–308.

Downes, H. (2001). Formation and modification of the shallow sub-continental lithospheric mantle: a review of geochemical evidence from ultramafic xenolith suites and tectonically emplaced ultramafic

massifs of Western and Central Europe. *Journal of Petrology* **42**, 233–350.

Elthon, D. (1992). Chemical trends in abyssal peridotites: refertilization of depleted suboceanic mantle. *Journal of Geophysical Research* **97**, 9015–9025.

Feigenson, M. D., Bolge, L. L., Carr, M. J. & Herzberg, C. T. (2003). REE inverse modeling of HSDP2 basalts: evidence for multiple sources in the Hawaiian plume. *Geochemistry, Geophysics, Geosystems* **4**(2), 8706, doi: 10.1029/2001GC000271.

Fitton, J. G. & Godard, M. (2004). Origin and evolution of magmas on the Ontong Java Plateau. In: Fitton, F. G., Mahoney, J., Wallace, P. & Saunders, A. (eds) *Origin and Evolution of the Ontong Java Plateau. Geological Society, London, Special Publications*, in press.

Francis, D. M. (2003). Cratonic mantle roots, remnants of a more chondritic Archean mantle? *Lithos* **71**, 135–152.

Francis, D. M., Hynes, A. J., Ludden, J. N. & Bédard, J. (1981). Crystal fractionation and partial melting in the petrogenesis of a Proterozoic high-MgO volcanic suite, Ungava, Quebec. *Contributions to Mineralogy and Petrology* **78**, 27–36.

Francis, D. M., Ludden, J. N. & Hynes, A. J. (1983). Magma evolution in a Proterozoic rifting environment. *Journal of Petrology* **24**, 556–582.

Frey, F. A. & Prinz, M. (1978). Ultramafic inclusions from San Carlos, Arizona: petrologic and geochemical data bearing on their petrogenesis. *Earth and Planetary Science Letters* **38**, 129–176.

Frey, F. A., Suen, C. J. & Stockman, H. W. (1985). The Ronda high temperature peridotite: geochemistry and petrogenesis. *Geochimica et Cosmochimica Acta* **49**, 2469–2491.

Godard, M., Jousselin, D. & Bodinier, J.-L. (2000). Relationships between geochemistry and structure beneath a paleo-spreading centre: a study of the mantle section in the Oman ophiolite. *Earth and Planetary Science Letters* **180**, 133–148.

Griffin, W. L., Smith, D., Boyd, F. R., Cousens, D. R., Ryan, C. G., Sie, S. H. & Suter, G. F. (1989). Trace-element zoning in garnets from sheared mantle xenoliths. *Geochimica et Cosmochimica Acta* **53**, 561–567.

Grove, T. L., Parman, S. W. & Dann, J. C. (1999). Conditions of magma generation for Archean komatiites from the Barberton Mountainland, South Africa. In: Fei, Y., Bertka, C. & Mysen, B. O. (eds) *Mantle Petrology: Field Observations and High Pressure Experimentation: a Tribute to Francis R. (Joe) Boyd. Geochemical Society Special Publication* **6**, 155–167.

Hanghøj, K., Kelemen, P., Bernstein, S., Blusztajn, J. & Frei, R. (2001). Osmium isotopes in the Wiedemann Fjord mantle xenoliths: a unique record of cratonic mantle formation by melt depletion in the Archean. *Geochemistry, Geophysics, Geosystems* **2**, paper number 2000GC000085.

Hanson, G. N. & Langmuir, C. H. (1978). Modelling of major elements in mantle–melt systems using trace element approaches. *Geochimica et Cosmochimica Acta* **42**, 725–741.

Herzberg, C. (1992). Depth and degree of melting of komatiites. *Journal of Geophysical Research* **97**, 4521–4540.

Herzberg, C. T. (1993). Lithosphere peridotites of the Kaapvaal craton. *Earth and Planetary Science Letters* **120**, 13–29.

Herzberg, C. (1999). Phase equilibrium constraints on the formation of cratonic mantle. In: Fei, Y., Bertka, C. & Mysen, B. O. (eds) *Mantle Petrology: Field Observations and High Pressure Experimentation: a Tribute to Francis R. (Joe) Boyd. Geochemical Society Special Publication* **6**, 241–257.

Herzberg, C. (2004*a*). Partial melting below the Ontong Java Plateau. In: Fitton, G., Mahoney, J., Wallace, P. & Saunders, A. (eds) *Origin and Evolution of the Ontong Java Plateau. Geological Society, London, Special Publications*, in press.

Herzberg, C. (2004*b*). Partial crystallization of mid-ocean ridge basalts in the crust and mantle. *Journal of Petrology* **45**, 2389–2406.

Herzberg, C. & O'Hara, M. J. (1998). Phase equilibrium constraints on the origin of basalts, picrites, and komatiites. *Earth-Science Reviews* **44**, 39–79.

Herzberg, C. & O'Hara, M. J. (2002). Plume-associated ultramafic magmas of Phanerozoic age. *Journal of Petrology* **43**, 1857–1883.

Herzberg, C. & Zhang, J. (1996). Melting experiments on anhydrous peridotite KLB-1: compositions of magmas in the upper mantle and transition zone. *Journal of Geophysical Research* **101**, 8271–8295.

Hynes, A. J. & Francis, D. M. (1982). A transect of the early Proterozoic Cape Smith foldbelt, New Quebec. *Tectonophysics* **88**, 23–59.

Iwamori, H., McKenzie, D. & Takahashi, E. (1995). Melt generation by isentropic mantle upwelling. *Earth and Planetary Science Letters* **134**, 253–266.

Johnson, K. T. M. & Dick, H. J. B. (1992). Open system melting and the temporal and spatial variation of peridotite and basalt compositions at the Atlantis II F.Z. *Journal of Geophysical Research* **97**, 9219–9241.

Johnson, K. T. M., Dick, H. J. B. & Shimizu, N. (1990). Melting in the oceanic upper mantle: an ion microprobe study of diopsides in abyssal peridotites. *Journal of Geophysical Research* **95**, 2661–2678.

Jordan, T. H. (1978). Composition and development of the continental tectosphere. *Nature* **274**, 544–548.

Jordan, T. H. (1988). Structure and formation of the continental tectosphere. *Journal of Petrology, Special Lithosphere Issue*, 11–37.

Kelemen, P. B., Dick, H. J. B. & Quick, J. E. (1992). Formation of harzburgite by pervasive melt/rock reaction in the upper mantle. *Nature* **358**, 635–641.

Kelemen, P. B., Hart, S. R. & Bernstein, S. (1998). Silica enrichment in the continental upper mantle via melt/rock reaction. *Earth and Planetary Science Letters* **164**, 387–406.

Kopylova, M. G. & Russell, J. K. (2000). Chemical stratification of cratonic lithosphere: constraints from the northern Slava craton, Canada. *Earth and Planetary Science Letters* **181**, 71–87.

Kuno, H. & Aoki, K. (1970). Chemistry of ultramafic nodules and their bearing on the origin of basaltic magmas. *Physics of the Earth and Planetary Interiors* **3**, 273–301.

Lahaye, Y. & Arndt, N. (1996). Alteration of a komatiite flow from Alexo, Ontario, Canada. *Journal of Petrology* **37**, 1261–1284.

Langmuir, C. H., Klein, E. M. & Plank, T. (1992). Petrology systematics of mid-ocean ridge basalts: constraints on melt generation beneath ocean ridges. In: Phipps Morgan, J., Blackman, D. K. & Sinton, J. M. (eds) *Mantle Flow and Melt Generation at Mid-Ocean Ridges. Geophysical Monograph, American Geophysical Union* **71**, 183–280.

Laurora, A., Mazzucchelli, M., Rivalenti, G., Vannucci, R., Zanetti, A., Barbieri, M. A. & Cingolani, C. A. (2001). Metasomatism and melting in carbonated peridotite xenoliths from the mantle wedge: the Gobernador Gregores Case (Southern Patagonia). *Journal of Petrology* **42**, 69–87.

Lécuyer, C. & Ricard, Y. (1999). Long-term fluxes and budget of ferric iron: implication for the redox states of the Earth's mantle and atmosphere. *Earth and Planetary Science Letters* **165**, 197–211.

Lécuyer, C., Gruau, G., Anhaeusser, C. R. & Fourcade, S. (1994). The origin of fluids and the effects of metamorphism on the primary chemical compositions of Barberton komatiites: new evidence from geochemical (REE) and isotopic (Nd, O, H, $^{39}Ar/^{40}Ar$) data. *Geochimica et Cosmochimica Acta* **58**, 969–984.

Lee, C.-T. & Rudnick, R. L. (1999). Compositionally stratified cratonic lithosphere: petrology and geochemistry of peridotite xenoliths from the Labait volcano, Tanzania. In: Gurney, J. J., Gurney, J. L., Pascoe, M. D. & Richardson, S. H. (eds) *Proceedings of the*

7th International Kimberlite Conference. Cape Town: Red Roof Design, pp. 503–521.

Lee, C.-T., Brandon, A. D. & Norman, M. (2003). Vanadium in peridotites as a proxy for paleo-fO_2 during partial melting: prospects, limitations, and implications. *Geochimica et Cosmochimica Acta* **67**, 3045–3064.

Lesher, C. M. & Arndt, N. T. (1995). REE and Nd isotope geochemistry, petrogenesis and volcanic evolution of contaminated komatiites at Kambalda, Western Australia. *Lithos* **34**, 127–157.

Lippard, S. J., Shelton, A. W. & Gass, I. G. (1986). *The Ophiolite of Northern Oman*. *Geological Society*, *London*, *Memoirs* **11**, 178 pp.

Maaloe, S. & Aoki, K.-i. (1977). The major element composition of the upper mantle estimated from the composition of lherzolites. *Contributions to Mineralogy and Petrology* **63**, 161–173.

Maury, R. C., Defant, M. J. & Joron, J.-L. (1992). Metasomatism of the sub-arc mantle inferred from trace elements in Philippine xenoliths. *Nature* **360**, 661–663.

McDonough, W. F. & Sun, S.-s. (1995). The composition of the Earth. *Chemical Geology* **120**, 223–253.

McInnes, B. I. A., Gregoire, M., Binns, R. A., Herzig, P. M. & Hannington, M. D. (2001). Hydrous metasomatism of oceanic sub-arc mantle, Lihir, Papua New Guinea: petrology and geochemistry of fluid-metasomatised mantle wedge xenoliths. *Earth and Planetary Science Letters* **188**, 169–183.

McKenzie, D. (1984). The generation and compaction of partial melts. *Journal of Petrology* **25**, 713–765.

McKenzie, D. & Bickle, M. J. (1988). The volume and composition of melt generated by extension of the lithosphere. *Journal of Petrology* **29**, 625–679.

Menzies, M. & Allen, C. (1974). Plagioclase lherzolite–residual mantle relationships within two Eastern Mediterranean ophiolites. *Contributions to Mineralogy and Petrology* **45**, 197–213.

Neal, C. R., Mahoney, J. J., Kroenke, L. W., Duncan, R. A. & Pettersen, M. G. (1997). The Ontong Java Plateau. In: Mahoney, J. J. & Coffin, M. L. (eds) *Large Igneous Provinces*. *Geophysical Monograph, American Geophysical Union* **100**, 183–216.

Nesbitt, R. W., Sun, S.-s. & Purvis, A. C. (1979). Komatiites: geochemistry and genesis. *Canadian Mineralogist* **17**, 165–186.

Nisbet, E. G., Bickle, M. J. & Martin, A. (1977). The mafic and ultramafic lavas of the Belingwe Greenstone Belt, S. Rhodesia, *Journal of Petrology* **18**, 521–566.

Nisbet, E. G., Arndt, N. T., Bickle, M. J., Cameron, W. E., Chauvel, C., Cheadle, M., Hegner, A., Martin, A., Renner, R. & Roedder, E. (1987). Uniquely fresh 2·7 Ga old komatiites from the Belingwe Greenstone Belt, Zimbabwe. *Geology* **15**, 1147–1150.

Niu, Y. (1997). Mantle melting and melt extraction processes beneath ocean ridges: evidence from abyssal peridotites. *Journal of Petrology* **38**, 1047–1074.

Niu, Y. & O'Hara, M. J. (2003). Origin of ocean island basalts: a new perspective from petrology, geochemistry, and mineral physics considerations. *Journal of Geophysical Research* **108**(B4, ECV 5), 1–19.

Niu, Y., Langmuir, C. H. & Kinzler, R. J. (1997). The origin of abyssal peridotites: a new perspective. *Earth and Planetary Science Letters* **152**, 251–265.

Niu, Y., O'Hara, M. J. & Pearce, J. A. (2003). Initiation of subduction zones as a consequence of lateral compositional buoyancy contrast within the lithosphere: a petrological perspective. *Journal of Petrology* **44**, 851–866.

Nixon, P. H. & Boyd, F. R. (1973). Petrogenesis of the granular and sheared ultrabasic nodule suite. In Nixon, P. H. (ed.) *Lesotho Kimberlites*. Maseru: Lesotho National Development Corporation, pp. 48–56.

O'Hara, M. J., Saunders, M. J. & Mercy, E. P. L. (1975). Garnet-peridotite, primary ultrabasic magma and eclogite; interpretation of upper mantle processes in kimberlite. *Physics and Chemistry of the Earth* **9**, 571–604.

Ohtani, E., Suzuki, A. & Kato, T. (1998). Flotation of olivine and diamond in mantle melt at high pressure: implications for fractionation in the deep mantle and ultradeep origin of diamond. In: Manghnani, M. H. & Yagi, T. (eds) *Properties of Earth and Planetary Materials*. *Geophysical Monograph, American Geophysical Union* **101**, 227–239.

Parkinson, I. J. & Arculus, R. J. (1999). The redox state of subduction zones: insights from arc-peridotites. *Chemical Geology* **160**, 409–423.

Parkinson, I. J. & Pearce, J. A. (1998). Peridotites from the Izu–Bonin–Mariana forearc (ODP Leg 125): evidence for mantle melting and melt–mantle interaction in a supra-subduction zone setting. *Journal of Petrology* **39**, 1577–1618.

Parman, S. W., Dann, J. C., Grove, T. L. & de Wit, M. J. (1997). Emplacement conditions of komatiite magmas from the 3·49 Ga Komati Formation, Barberton Greenstone Belt, South Africa. *Earth and Planetary Science Letters* **150**, 303–323.

Pearce, J. A., Barker, P. F., Edwards, S. J., Parkinson, I. J. & Leat, P. T. (2000). Geochemistry and tectonic significance of peridotites from the South Sandwich arc–basin system, South Atlantic. *Contributions to Mineralogy and Petrology* **139**, 36–53.

Pearson, D. G., Shirey, S. B., Carlson, R. W., Boyd, F. R. Pokhilenko, N. P. & Shimizu, N. (1995). Re–Os, Sm–Nd, and Rb–Sr isotope evidence for thick Archean lithosphere mantle beneath the Siberian craton modified by multistage metasomatism. *Geochimica et Cosmochimica Acta* **59**, 959–978.

Picard, C. (1989). *Lithochimie des roches volcaniques protérozoïques de la partie occidentale de la Fosse de l'Ungava, région au sud du lac Lanyan*. Charlesbourg, Que.: Ministère de l'Énergie et des Ressources, Québec, ET 87-14, 73 pp.

Picard, C., Lamothe, D., Piboule, M. & Oliver, R. (1990). Magmatic and geotectonic evolution of a Proterozoic oceanic basin system: the Cape Smith thrust–fold belt (New-Quebec). *Precambrian Research* **47**, 223–249.

Pollack, H. N. (1997). Thermal characteristics of the Archaean. In: de Wit, M & Ashwall, L. D. (eds) *Greenstone Belts*. *Oxford Monographs on Geology and Geophysics* **35**, 223–232.

Reisberg, L. & Lorand, J.-P. (1995). Longevity of sub-continental mantle lithosphere from osmium isotope systematics in orogenic peridotite massifs. *Nature* **376**, 159–162.

Renner, R., Nisbet, E. G., Cheadle, M. J., Arndt, N. T., Bickle, M. J. & Cameron, W. E. (1994). Komatiite flows from the Reliance Formation, Belingwe belt, Zimbabwe: I. Petrography and mineralogy. *Journal of Petrology* **35**, 361–400.

Robertson, A. H. F. (2002). Overview of the genesis and emplacement of Mesozoic ophiolites in the Eastern Mediterranean Tethyan region. *Lithos* **65**, 1–67.

Saunders, A. D., Fitton, J. G., Kerr, A. C., Norry, M. J. & Kent, R. W. (1997). The North Atlantic Igneous Province. In: Mahoney, J. J. & Coffin, M. L. (eds) *Large Igneous Provinces*. *Geophysical Monograph, American Geophysical Union* **100**, 45–93.

Schmidberger, S. S. & Francis, D. (2001). Constraints on the trace element composition of the Archean mantle root beneath Somerset Island, Arctic Canada. *Journal of Petrology* **42**, 1095–1117.

Sen, G. (1987). Xenoliths associated with the Hawaiian hot spot. In: Nixon, P. H. (ed.) *Mantle Xenoliths*. New York: John Wiley, pp. 359–375.

Seyler, M., Cannat, M. & Mével, C. (2003). Evidence for major-element heterogeneity in the mantle source of abyssal peridotites

from the Southwest Indian Ridge (52° to 68°E). *Geochemistry, Geophysics, Geosystems* **4**, paper number 2002GC000305.

Simon, N. S. C., Irvine, G. J., Davies, G. R., Pearson, D. G. & Carlson, R. W. (2003). The origin of garnet and clinopyroxene in 'depleted' Kaapvaal peridotites. *Lithos* **71**, 289–322.

Smith, D. & Boyd, F. R. (1987). Compositional heterogeneities in a high-temperature lherzolite nodule and implications for mantle processes. In: Nixon, P. H. (ed.) *Mantle Xenoliths*. New York: John Wiley, pp. 551–561.

Smith, D., Riter, J. C. A. & Mertzmann, S. A. (1999). Water–rock interactions, orthopyroxene growth, and Si-enrichment in the mantle: evidence in xenoliths from the Colorado Plateau, southwestern United States. *Earth and Planetary Science Letters* **165**, 45–54.

Smith, H. S. & Erlank, A. J. (1982). Geochemistry and petrogenesis of komatiites from the Barberton greenstone belt, South Africa. In: Arndt, N. T. & Bickle, E. G. (eds) *Komatiites*. London: Allen and Unwin, pp. 347–397.

Snow, J. E. & Dick, H. J. B. (1995). Pervasive magnesium loss by marine weathering of peridotite. *Geochimica et Cosmochimica Acta* **59**, 4219–4235.

Sproule, R. A., Lesher, C. M., Ayer, J. A., Thurston, P. C. & Herzberg, C. T. (2002). Spatial and temporal variations in the geochemistry of komatiites and komatiitic basalts in the Abitibi greenstone belt. *Precambrian Research* **115**, 153–186.

Sun, S.-S. & Nesbitt, R. W. (1978). Petrogenesis of Archaean ultrabasic and basic volcanics: evidence from rare earth elements. *Contributions to Mineralogy and Petrology* **65**, 301–325.

Takahashi, E. (1990). Speculations on the Archean mantle: missing link between komatiite and depleted garnet peridotite. *Journal of Geophysical Research* **95**, 15941–15954.

Takazawa, E., Okayasu, T. & Satoh, K. (2003). Geochemistry and origin of the basal lherzolites from the northern Oman ophiolite (northern Fizh block). *Geochemistry, Geophysics, Geosystems* **4**, 2001GC000232.

Viljoen, R. P. & Viljoen, M. J. (1969). Evidence for the composition of the primitive mantle and its products of partial melting from a study of the rocks of the Barberton Mountain Land. *Geological Society of South Africa, Special Publication* **2**, 275–296.

Walter, M. J. (1998). Melting of garnet peridotite and the origin of komatiite and depleted lithosphere. *Journal of Petrology* **39**, 29–60.

Wood, B. J., Bryndzia, L. T. & Johnson, K. E. (1990). Mantle oxidation state and its relationship to tectonic enviroment and fluid speciation. *Science* **248**, 337–345.

Yang, H.-J., Sen, G. & Shimizu, N. (1998). Mid-ocean ridge melting: constraints from lithospheric xenoliths at Oahu, Hawaii. *Journal of Petrology* **39**, 277–295.